

FABRICATION OF A SUPERHYDROPHOBIC AND OLEOPHILIC FILTER FOR EFFECTIVE SEPARATION OF OIL- WATER MIXTURES

by

Natchaya Kaewma

A Thesis Submitted in Partial Fulfillment of the Requirements for the Degree of
Master of Engineering in Bio-Nano Material Science and Engineering

Examination Committee: Dr. Tanujjal Bora (Chairperson)
Dr. Raffaele Ricco
Prof. Dieter Wilhelm Trau

Nationality: Thai
Previous Degree: Bachelor of Engineering in Mechanical
Engineering
Chiang Mai University
Chiang Mai, Thailand

Scholarship Donor: His Majesty the King's Scholarships
(Thailand)

Asian Institute of Technology
School of Engineering and Technology
Thailand
May 2024

AUTHOR'S DECLARATION

I, Natchaya Kaewma, declare that the research work carried out for this thesis was in accordance with the regulations of the Asian Institute of Technology. The work presented in it is my own and has been generated by me as the result of my own original research, and if external sources were used, such sources have been cited. It is original and has not been submitted to any other institution to obtain another degree or qualification. This is a true copy of the thesis, including final revisions.

Date: April 30th, 2024

Name (in printed letters): NATCHAYA KAEWMA

Signature: Natchaya Kaewma

ACKNOWLEDGMENTS

I would like to express my sincere gratitude to my advisor, Dr. Tanujjal Bora, for his invaluable guidance, support, and encouragement throughout my research journey. His suggestions and assistance have been instrumental in shaping my research questions, methodology, and analysis. I would also like to extend my gratitude to Dr. Raffaele Ricco, who served as the committee member for my thesis. His useful advice and feedback have greatly improved the quality of my work. I am also grateful to Dr. Dieter Trau for providing me with the important equipment that was necessary for my experiment. Their support has been crucial to the success of my research. My sincere thanks go to His Majesty the King's Scholarships for providing me with the necessary funding to carry out my study at AIT. Without this financial support, my studies would not have been possible. Finally, I would like to express my heartfelt thanks to my family and AIT friends for their support and encouragement throughout this journey. Their mental and emotional support have been invaluable to me.

ABSTRACT

This study investigates the development and performance of a superhydrophobic stainless steel mesh modified with a polydimethylsiloxane-silica (PDMS-SiO₂) nanocomposite coating. The coated mesh exhibited exceptional water repellency, with water contact angles exceeding 150° compared to uncoated meshes and pure PDMS coatings. Moreover, the mesh coated with PDMS-SiO₂ has a sliding angle value as low as 7°, showing excellent self-cleaning properties. Durability tests revealed the superior mechanical resilience of the PDMS-SiO₂ coating compared to other mesh types. Chemical stability analysis demonstrated minimal influence of pH on their hydrophobicity, indicating consistent performance under various environmental conditions. The self-cleaning test highlighted the remarkable ability of PDMS-SiO₂ mesh to remove various contaminants due to their superhydrophobic and low surface energy properties. Conversely, uncoated, and pure PDMS meshes exhibited limited self-cleaning capabilities. Finally, the efficiency test explored the effectiveness of these meshes in separating water from different oil types. The results suggest that both coating volume and the specific oil type influence separation performance, indicating the potential for optimization based on the targeted oil. Overall, this research demonstrates the promising potential of PDMS-SiO₂ coated stainless steel mesh for various applications requiring durability, self-cleaning functionality, and efficient oil-water separation.

CONTENTS

	Page
AUTHOR'S DECLARATION	ii
ACKNOWLEDGEMENTS	iii
ABSTRACT	iv
LIST OF TABLES	viii
LIST OF FIGURES	ix
LIST OF ABBREVIATIONS	xi
CHAPTER 1 INTRODUCTION	1
1.1 Background of the Study	1
1.2 Statement of the Problem	3
1.3 Research Questions	3
1.4 Objectives of the Study	4
1.5 Scope of Study	4
CHAPTER 2 LITERATURE REVIEW	5
2.1 Basic Theories of Oil–Water Separation	5
2.2 Surface Wettability	6
2.2.1 The Role of Wettability in Solid Surface Properties	7
2.2.2 Surface Energy	7
2.2.3 Surface Tension	8
2.3 Wetting Models on a Solid Surface	10
2.3.1 Young's Model	10
2.3.2 Wenzel State	11
2.3.3 Cassie-Baxter State	13
2.4 Synthesis Techniques for Creating Superhydrophobic Surfaces	14
2.4.1 Electrochemical Deposition Technique	15
2.4.2 Plasma-Etching Technique	15
2.4.3 Photolithography Technique	16
2.4.4 Dip Coating Technique	17
2.4.5 Spray Coating Technique	18
2.5 PDMS-Based Filter for Superhydrophobic Surface in Oil-Water Separation	19

	Page
2.5.1 PDMS-Based Filter Design	19
2.5.2 PDMS-Based Filter Design	19
2.5.3 Durability and Stability	19
2.5.4 Application Potential	20
2.6 Previous Research Works on Superhydrophobic Surfaces	20
2.6.1 Ge et al.(2014)	20
2.6.2 Wu et al.(2017)	21
2.6.3 Li et al.(2018)	21
2.6.4 Xiao Gong and Shuang He(2020)	21
2.7 Chapter Summary	22
CHAPTER 3 METHODOLOGY	23
3.1 Cleaning Stainless Steel Mesh	23
3.2 Preparation of PDMS-SiO ₂ Composites	24
3.3 Preparation of Superhydrophobic Mesh on the Substrate	
Mesh by Spray Coating	24
3.4 Characterization of the Superhydrophobic Mesh	25
3.4.1 Scanning Electron Microscope	25
3.4.2 Contact Angle Measurement	26
3.4.3 Sliding Angle Measurement	27
3.5 Durability Test	28
3.6 Chemical Stability Test	29
3.7 Self-Cleaning Ability Test	30
3.8 Oil-Water Separation Apparatus Fabrication	31
3.9 Efficiency of Oil-Water Separation	32
CHAPTER 4 RESULTS AND DISCUSSIONS	34
4.1 Stainless-Steel Mesh Measurement	34
4.2 Surface Morphology	35
4.3 Surface Wetting Behavior	38
4.4 Evaluation of Oleophilic Behavior	40
4.5 Durability Test	42
4.6 pH stability Test	44
4.7 Self-Cleaning Test	45
4.8 Oil-Water Separation Test	49

	Page
CHAPTER 5 CONCLUSION	54
REFERENCES	56

LIST OF TABLES

Tables	Page
Table 4.1 Data of Water Inserted and Collected with Different Types of Oil & Their Respective Separation Efficiency	51

LIST OF FIGURES

Figures	Page
Figure 1.1 Number of Tanker Spills by Decade, 1970 – 2022	1
Figure 2.1 Oil-Water Separation Techniques	6
Figure 2.2 The Wettability of the Surface	7
Figure 2.3 Surface Tension of a Droplet	9
Figure 2.4 Surface Tension Measurements	10
Figure 2.5 Illustration Depicting Contact Angle Determination Using Young's equation	11
Figure 2.6 Illustration of the Wenzel State on a Highly Wetting Surface	12
Figure 2.7 Illustration of Static and Dynamic Contact Angles	12
Figure 2.8 Visual Depiction of a Composite Liquid-Vapor Interface for Cassie-Baxter State	13
Figure 2.9 Illustration of the Electrochemical Deposition Setup	15
Figure 2.10 Schematic Showing the Key Components for Plasma Etching	16
Figure 2.11 Diagrammatic Representation of Photolithographic Patterning	17
Figure 2.12 Visual Depiction of the Steps Involved in Dip Coating	18
Figure 2.13 Schematic Diagram of the Spray Coating Technique	18
Figure 3.1 Stainless-Steel Mesh Clean Process	23
Figure 3.2 PDMS-SiO ₂ Composites Preparation	24
Figure 3.3 Spray Coating Technique for the Superhydrophobic Mesh Fabrication	25
Figure 3.4 Contact Angle Measurement Process	26
Figure 3.5 Experiment Setup for Sliding Angle Measurement	27
Figure 3.6 Durability Testing of the Mesh	28
Figure 3.7 Preparation of Water with a pH of 3-13 by Using Hydrochloric Acid and Sodium Hydroxide	29
Figure 3.8 Self-Cleaning Ability Testing of the Mesh	31
Figure 3.9 Schematic Showing the Components Involved in the Oil-Water Separation Process	31
Figure 3.10 The Process of Water and Oil Filtration	33
Figure 4.1 Stainless 304 Wire Mesh Filter 200 Mesh-75 Micron	35

Figures	Page
Figure 4.2 SEM Micrographs of Uncoated and Coated Mesh	36
Figure 4.3 Images Showing Water Droplet Sitting on the Coated and Uncoated Stainless-Steel Surfaces	39
Figure 4.4 The Image Shows the Sliding Angle of Each Surface	40
Figure 4.5 Images of Oil Contact Angle Measurements with Different of Oils	41
Figure 4.6 Variations in Oil Contact Angles on Uncoated and Coated Stainless-Steel Mesh	41
Figure 4.7 Changes in Water Repellency of the Mesh Observed after a Durability Test	43
Figure 4.8 Influence of Solution Acidity (pH 3-13) on the Wettability of Different Samples as Measured by Water Contact Angle	44
Figure 4.9 Amount of Substance on the Sample Surface after Self-Cleaning Test of Each Sample	46
Figure 4.10 Self-Cleaning Test on Uncoated Surface Mesh	47
Figure 4.11 Self-Cleaning Test on Pure PDMS Surface Mesh	48
Figure 4.12 Self-Cleaning Test on PDMS-SiO ₂ Surface Mesh	49
Figure 4.13 Experiment Setup for Oil-Water Separation	50
Figure 4.14 Still photographs of Water and Oil Being Separated Through a PDMS-SiO ₂ Coated Stainless-Steel Mesh	50
Figure 4.15 Influence of PDMS-SiO ₂ Coating on the Oil-Water Separation Capacity of Meshes	52

LIST OF ABBREVIATIONS

APTES = (3-Aminopropyl)triethoxysilane

DI-water = Deionized Water

HCl = Hydrochloric Acid

NaOH = Sodium Hydroxide

PDMS = Polydimethylsiloxane

PTES = Phenyltriethoxysilane

SEM = Scanning Electron Microscope

SSM = Stainless-Steel Mesh

UV = Ultraviolet

CHAPTER 1

INTRODUCTION

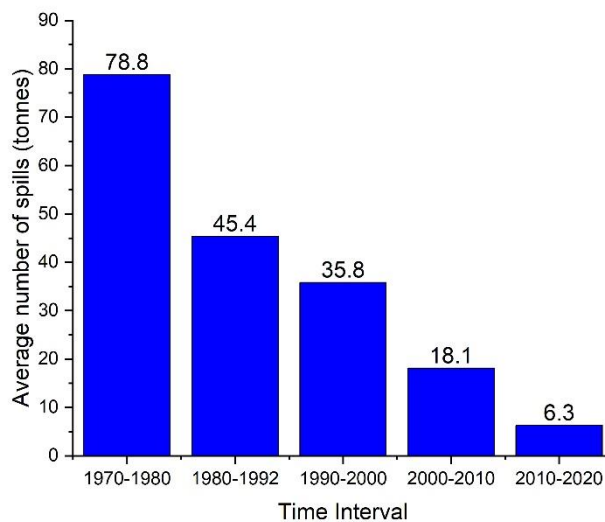
1.1 Background of the Study

In 2022, there were three major oil spill incidents, each involving over 700 tons of oil, and four intermediate-sized spills ranging from 7 to 700 tons. The data revealed a regional disparity in oil spill incidents, with two significant spills occurring in Asia and one in Africa. Intermediate-sized spills were scattered across North America, Asia, and Africa. This data suggests an average of nearly six oil spills exceeding 7 tons annually over the decade. The total oil volume released due to tanker spills in 2022 was estimated at 15,000 tons, with over 14,000 tons attributed to the three major incidents (ITOPF, 2024).

Over the past fifty years, there has been a noticeable and substantial decline in oil spills exceeding 7 tons from oil tankers, as illustrated in Fig 1.1 below. An average of roughly 79 oil spills took place each year throughout the 1970s., which decreased by over 90% to only 6 incidents by 2010. This trend has persisted into the current decade. However, despite the reduced frequency of spills, their environmental impact remains significant (ITOPF, 2024).

Figure 1.1

Number of Tanker Spills by Decade, 1970 - 2022



Note. Decades worth of data (1970-2022) allow for examining the frequency of medium-sized (7-700 tonnes) and large (>7 tonnes) spills from tankers. Note that there is limited data available for the 2020s, spanning only three years.

Marine oil spill responses often involve the use of chemical dispersants, a widely documented practice in both news reports and official protocols. Dispersants promote oil spill remediation by weakening the cohesive forces between oil molecules, lowering the surface tension of the oil slick, causing it to disperse. This leads to the creation of droplets or particles that sink beneath the sea surface (ITOPF, 2024).

In deep and turbulent waters, dispersants aid in the natural breakdown of oil by bacteria, safeguarding marine ecosystems. However, near coastlines (within 5 kilometers), dispersants may not disperse sufficiently, leading to concentrated underwater oil masses. This can harm seagrass beds, coral reefs, and marine biodiversity, as well as pollute beach areas, impacting tourist destinations (ITOPF, 2024).

Nonetheless, in the presence of contaminants within the marine environment, the primary and most immediately impacted category of organisms comprises aquatic animals, notably fish, which may ingest or meet specific oil varieties. While these aquatic animals may not succumb to immediate mortality, they frequently accumulate noxious substances in their liver and other organs (ITOPF, 2024).

In terms of human health, it is evident that marine animals form a significant portion of our diet. When these animals are exposed to toxins, consuming them essentially means ingesting these toxins. This sets off a cycle that leads to the gradual accumulation and retention of these harmful substances in our bodies over time (ITOPF, 2024).

From an environmental perspective, the short-term repercussions encompass a reduction in tourism, the implementation of commercial fishing restrictions, and the immediate impact on affected communities. In the long term, the natural environment, burdened by pollution, experiences a progressive deterioration. The traditional way of life for those reliant on this environment undergoes alteration, and unless comprehensive restoration and mitigation efforts are enacted, there looms a potential risk of extinction for the species that once thrived in this ecosystem (ITOPF, 2024).

The use of chemical dispersants results in the presence of harmful residual chemicals, accompanied by a significant financial expense and adverse environmental effects. This study aims to develop a cost-effective and simple surface model for separating water from oil. The model incorporates nanoparticles and organic compounds, providing a prototype for efficient oil filtration from water. This contribution aims to mitigate the negative consequences of oil spills (Zhu et al., 2022).

1.2 Statement of the Problem

Oil spills in marine environments threaten ecosystems and human well-being. Even smaller spills have severe environmental consequences. Conventional chemical dispersants leave residual chemicals, incurring high costs. Near coastlines, concentrated underwater oil masses harm marine life, seagrass beds, coral reefs, and tourist destinations.

Humans face health risks from consuming contaminated marine animals, and communities dependent on tourism and fishing suffer economic impacts. The current response with dispersants lacks sustainability in oil-water separation, demanding cost-effective alternatives.

In terms of oil-water separation, several research studies are ongoing providing various solutions to design effective filters or membranes to separate oil from water (Zhang et al., 2020, 2022). However, most of these techniques are either complex with high manufacturing and operation costs, or they show poor material stability. Hence, simple and effective filter development for this purpose is essential.

This research aims to develop a cost-effective superhydrophobic and oleophilic filter through spray-coating a PDMS/SiO₂ nanocomposite on stainless steel mesh. It addresses the limitations of chemical dispersants, offering a sustainable oil spill cleanup solution.

1.3 Research Questions

Considering the existing challenges posed by complex and expensive filtration systems, this research seeks to address two fundamental questions aimed at revolutionizing filtration technology:

1. How can we create or design a filter that is very simple to build and affordable than filters created in the past?
2. Can simple and cost-effective superhydrophobic filters effectively separate oil from water?

1.4 Objectives of the Study

The primary objective of this study is to create a filter membrane exhibiting both superhydrophobicity and oleophilicity, facilitating a highly efficient separation process for oil-water mixtures.

The research is guided by the following specific objectives:

1. To synthesize a composite based on PDMS that demonstrates pronounced superhydrophobic and oleophilic characteristics.
2. To modify a stainless-steel mesh using the PDMS-based composite, resulting in the creation of an advanced oil-water filter.
3. To construct and assess the performance of a laboratory-scale prototype of the oil-water filtration system, evaluating its effectiveness in achieving the desired separation.

1.5 Scope of Study

This research encompasses a comprehensive investigation into the fabrication, characterization, and application of a superhydrophobic stainless-steel mesh (SSM) coated with a PDMS-SiO₂ nanocomposite. The study involves a meticulous methodology for cleaning the SSM, synthesizing the nanocomposite, and employing a spray coating technique. The effectiveness of the superhydrophobic mesh is assessed through detailed characterization using scanning electron microscopy (SEM), contact angle measurements, and sliding angle measurement. The durability of the coating is examined through tape peeling tests, while its self-cleaning ability is demonstrated using sand, soil, dust, and graphite. Moreover, the sample was tested with acid and base water which has a pH of 3-13. Furthermore, the study extends to the design and fabrication of an oil-water separation apparatus, evaluating its efficiency in separating various oil-water mixtures. The research aims to contribute valuable insights into the development of robust, self-cleaning, and efficient materials for applications in oil-water separation and other relevant fields.

CHAPTER 2

LITERATURE REVIEW

Recently, scientists have developed surfaces that strongly repel water (superhydrophobic). This is a game-changer for separating oil from water, which is important for cleaning up spills and in many industrial processes. This section explains how these surfaces work and how they're made. We will also look at a special filter made from a material called PDMS that uses these superhydrophobic properties to separate oil and water very effectively. Finally, we'll discuss what other scientists have done in this field and how their ideas could be used in the real world. These developments are a big step forward in solving the problem of oil-water separation.

2.1 Basic Theories of Oil–Water Separation

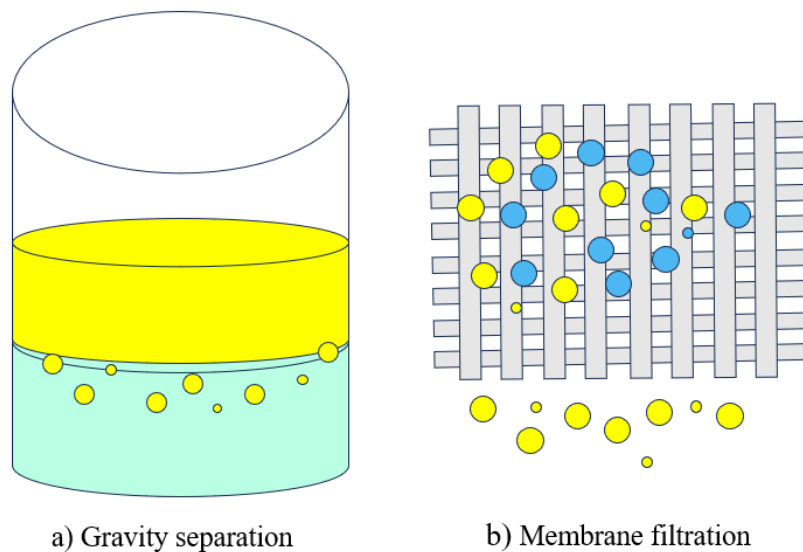
The oil-water separation process plays a pivotal role in the effective segregation of water and oil phases within mixtures or emulsions. This procedure serves a multitude of vital objectives, encompassing the retrieval of valuable resources, the mitigation of environmental contamination, and the facilitation of responsible disposal or reutilization of these non-miscible liquids (Chu et al., 2015; Gupta et al., 2017; Wang et al., 2021).

As the droplet size in these mixtures diminishes, the innate separation process experiences a reduction in its efficacy. Therefore, there is a critical need to explore and develop more advanced techniques and materials to achieve superior oil-water separation performance. Although traditional methods such as gravity separation (as depicted in Fig 2.1) and centrifugation incorporate a blend of physical, chemical, and biological mechanisms, they are constrained by drawbacks such as reduced efficiency and the inadvertent generation of secondary pollutants (Xue et al., 2014).

As shown in Figure 2.1, recent innovations in membrane filtration technology offer an effective method for purifying water and removing a wide range of pollutants, including persistent emulsions, dissolved oils, and chemical compounds(Xue et al., 2014).

Figure 2.1

Oil-Water Separation Techniques



Note. a) Gravity separation is a technique employed for the segregation of materials according to their varying densities, wherein heavier particles gravitate towards the lower regions, while lighter particles ascend to the upper layers. b) Membrane filtration is a process that separates particles and substances within a liquid by directing it through a semi-permeable membrane, enabling specific components to pass through while retaining others.

2.2 Surface Wettability

The wettability of a surface, characterized by the contact angle formed at the interface between a liquid droplet and the solid, constitutes a critical characteristic that governs the behavior of liquids on solids. This attribute can be categorized into four main classes: superhydrophilic, hydrophilic, hydrophobic, and superhydrophobic, with superhydrophobic surfaces typically achieved through surface roughness. Surface energy (γ) quantifies the energy required to generate a surface, while surface tension resists the expansion of surface area. These properties carry significant implications across a spectrum of fields, spanning from materials science to engineering, due to their profound impact on the interactions involving solids, liquids, and vapor.

2.2.1 The Role of Wettability in Solid Surface Properties

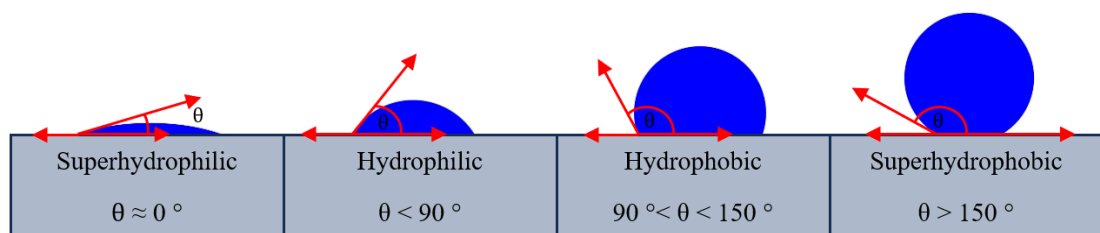
Wettability describes the inclination of a liquid to either disperse and cover a solid surface or form into beads, influenced by molecular interactions. Contact angle measurements are utilized to quantify and assess this property (Duta et al., 2015).

Solid surfaces can be classified into distinct wettability regimes based on the contact angle (θ) formed between a liquid droplet and the surface. Superhydrophilic surfaces ($\theta \approx 0^\circ$) exhibit complete wetting, while hydrophilic surfaces ($\theta < 90^\circ$) demonstrate partial wetting. Conversely, hydrophobic surfaces ($90^\circ < \theta < 150^\circ$) display partial nonwetting, and superhydrophobic surfaces ($\theta > 150^\circ$) exhibit complete nonwetting. Figure 2.2 illustrates these wettability categories (Kumar & Nanda, 2019).

Surface roughness plays a critical role in creating superhydrophobicity. By introducing roughness features, the behavior of water droplets on these surfaces can be significantly influenced (Kumar & Nanda, 2019).

Figure 2.2

The Wettability of the Surface



2.2.2 Surface Energy

The surface energy, denoted by γ , quantifies the energy required to create a unit area of a new surface. Usually presented in terms of $\text{N}\cdot\text{m}^{-1}$ (Tanujjal Bora, 2022). The atoms and molecules on the surface of solids exhibit similar properties to those in liquids, but they generally remain relatively immobile. In contrast to liquids, solids lack the capacity to spontaneously engage in chemical reactions or modify their shape to attain a lower-energy surface configuration. The equation below fundamentally relates the surface energy of a crystalline solid to its inherent properties.

$$E_s = \frac{1}{2} (N_s \epsilon_b) \dots\dots\dots \text{Equation 2. 1}$$

Where ϵ_b represents the cohesion or binding energy between pairs of atoms within the solid, and N_s denotes the quantity of atoms present in the surface layer. The factor of 1/2 is incorporated because the creation of a new surface involves the disruption of two bonds.

The contact angle, formed at the three-phase boundary (liquid, solid, and gas) where a liquid droplet meets a flat solid surface, can be used to estimate the surface energy of the solid. This intersection is regarded as a boundary condition. Young's equation, presented below, explains the relationship between surface tension and the forces acting at the liquid-vapor interface (Gabor L. Hornyak, 2008).

$$\cos\theta = \frac{\gamma_{SV}-\gamma_{SL}}{\gamma_{LV}} \dots\dots\dots \text{Equation 2. 2}$$

In Young's equation, θ represents the Young's contact angle, a measure of the interaction between a liquid droplet and a solid surface. γ_{SV} signifies the solid-vapor interfacial energy, while γ_{SL} represents the solid-liquid interfacial energy. Finally, γ_{LV} denotes the liquid-vapor interfacial energy (Kumar & Nanda, 2019).

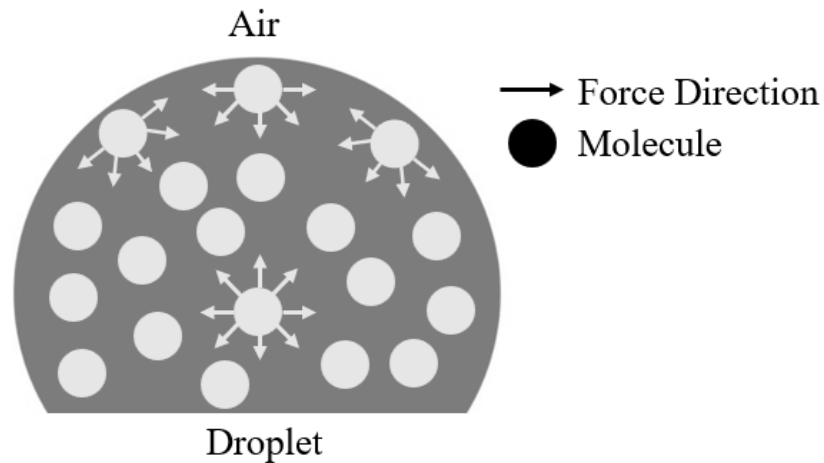
2.2.3 Surface Tension

Surface tension, measured in Newtons per meter (N/m), quantifies the contractile force acting at the liquid's surface that resists any increase in its area (Tanujjal Bora, 2022). Surface tension is influenced by a multitude of factors, including hydrogen bonding, particularly notable in water, as well as entropic effects, signifying that the surface tends to be more disordered than the bulk of the liquid (Gabor L. Hornyak, 2008).

Intermolecular forces between a droplet's constituent molecules dictate the magnitude of its surface tension. Molecules inside the droplet encounter intermolecular forces acting uniformly from all directions. However, at the surface of the droplet, there's an absence of liquid molecules on the exterior side. The molecules at the surface exhibit stronger intermolecular connections compared to those within the interior because they aren't subject to forces from all directions. This property renders it more challenging for an object to penetrate the surface in comparison to moving within the interior once submerged, as illustrated in Fig2.3 below (Gabor L. Hornyak, 2008).

Figure 2.3

Surface Tension of a Droplet

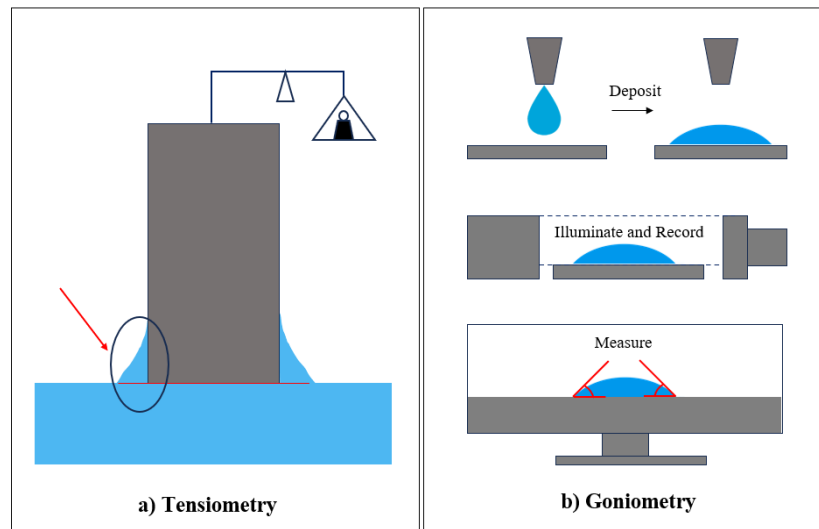


Note. Water molecules positioned at or near the surface encounter heightened lateral and inward forces, compelling them to contract. Conversely, water molecules situated nearer to the body's center experience an equilibrium of attractive and repulsive forces acting uniformly from all directions. The net effect of these interactions gives rise to the phenomenon of surface tension and an inherent propensity to reduce the surface area (Tanujjal Bora, 2022).

When it comes to measuring surface tension and energy, two primary methods are commonly employed: tensiometry, which relies on mechanical principles utilizing a calibrated probe, and contact angle goniometry, an optical approach. Tensiometry entails the use of a probe interacting with a liquid surface, as depicted in Fig 2.4a, while contact angle goniometry serves to independently verify the results, as shown in Fig 2.4b. To measure the surface energy of solids, the process entails the placement of liquids on the solid surface, recording contact angles, and subsequently calculating surface energy indirectly (Gabor L. Hornyak, 2008).

Figure 2.4

Surface Tension Measurements



2.3 Wetting Models on a Solid Surface

This chapter explores the fundamental principles of surface wettability. Key theoretical models, including Young's equation for smooth surfaces, the Wenzel state for rough surfaces, and the Cassie-Baxter state which considers trapped air pockets, will be examined. These models have significant applications in various fields, particularly material design, and the development of superhydrophobic surfaces.

2.3.1 Young's Model

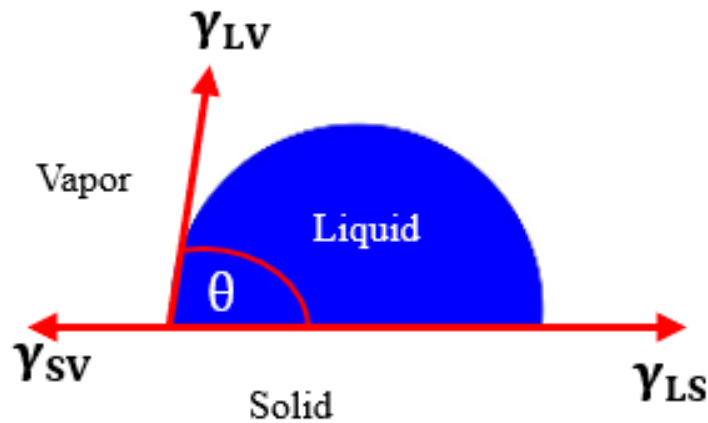
Considering a scenario where a liquid droplet rests on a perfectly smooth solid surface in an air environment, as illustrated in Figure 2.5, Young's equation (presented below) can be applied to calculate the contact angle formed between the liquid and the solid surface (Chen et al., 2019) as shown in below equation.

$$\cos\theta = \frac{\gamma_{SV}-\gamma_{SL}}{\gamma_{LV}} \dots\dots\dots \text{Equation 2. 3}$$

In the equation, which represents Young's equation, θ denotes the Young's contact angle, reflecting the interaction between a liquid droplet and a solid surface. γ_{SV} signifies the solid-vapor interfacial energy, while γ_{SL} represents the solid-liquid interfacial energy. Finally, γ_{LV} denotes the liquid-vapor interfacial energy (Kumar & Nanda, 2019).

Figure 2.5

Illustration Depicting Contact Angle Determination Using Young's Equation



Note. A schematic depicting Young's equation is shown below. The symbols represent: θ - the contact angle, γ_{LV} - the liquid's surface tension, γ_{SL} - the interfacial tension between solid and liquid, and γ_{SV} - the solid's surface free energy. (Units: $\text{mN/m} = \text{mJ/m}^2$)

2.3.2 Wenzel State

Superhydrophobic surfaces are fashioned by introducing roughness to solid surfaces, significantly influencing the behavior of water droplets. The Wenzel state defines these surfaces when there are no air pockets present between the rough features, as illustrated in Fig 2.6 (R.N. Wenzel, 1936). The Wenzel state, illustrated in Figure 2.7a, exhibits a decrease in static contact angle compared to a smooth surface. This is accompanied by an increase in the sliding angle, as shown in Figure 2.7b. The roughness of the surface traps droplets within its grooves, hindering their ability to slide easily. When the water is in motion, it results in dynamic contact angles during the movement of the droplet across the surface, as seen in Fig 2.7c. Understanding the interplay between surface roughness and contact angles is crucial for designing superhydrophobic surfaces with practical applications, including self-cleaning materials and water-repellent coatings.

Figure 2.6

Illustration of the Wenzel State on a Highly Wetting Surface

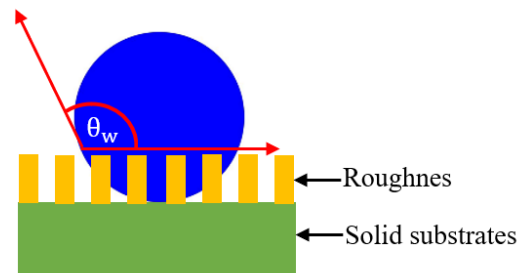
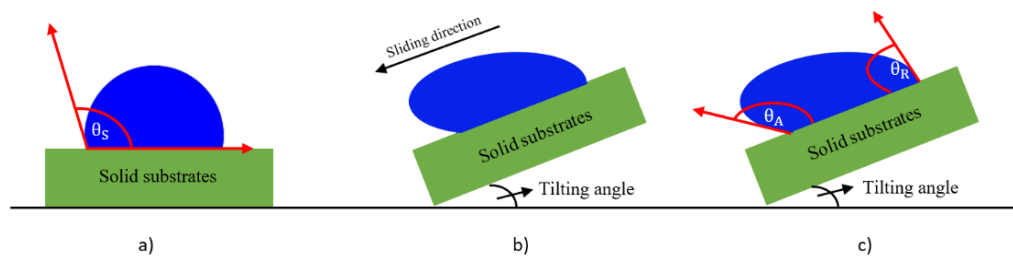


Figure 2.7

Illustration of Static and Dynamic Contact Angles



Note. a) The static contact angle is the angle measured between a liquid droplet and a solid surface when the droplet remains stationary, representing a stable equilibrium. b) The sliding angle is a critical threshold. It represents the tilt angle at which a liquid droplet resting on a surface initiates movement and begins to slide off. c) The dynamic contact angle captures the range of contact angles observed as a liquid droplet interacts with a surface. This includes the advancing angle (θ_{adv}) measured during the wetting process, where the droplet spreads, and the receding angle (θ_{rec}) measured during dewetting, where the droplet retracts (GmbH, 2012).

Young's equation, originally designed for ideal flat surfaces, does have limitations in its applicability. Recognizing this, Wenzel introduced a fresh perspective. He noted that the real surface area of a rough surface exceeds what would be expected on a smooth surface. As a result, he introduced a modified model that takes surface roughness into account, presenting an equation as described below (Kumar & Nanda, 2019).

$$\cos\theta_w = r \cos\theta \dots\dots\dots \text{Equation 2. 4}$$

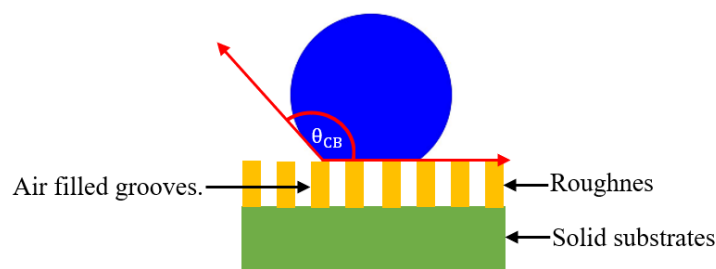
The Wenzel equation, expressed below, describes the relationship between the contact angle (θ_w) of a liquid droplet on a rough surface, the surface roughness (r), and the Young's contact angle (θ_Y) for a smooth surface. The roughness factor (r) represents the ratio of the actual surface area (accounting for roughness features) to the projected surface area (what appears smooth). For a perfectly smooth surface, the roughness factor is 1. Conversely, rough surfaces have roughness factors greater than 1. According to Wenzel's theory, for hydrophilic surfaces, increasing roughness generally enhances wettability, resulting in easier liquid spreading, while for hydrophobic surfaces, increased roughness can reduce wettability, causing droplets to bead up rather than spread (Kumar & Nanda, 2019).

2.3.3 Cassie-Baxter State

The Cassie-Baxter state provides an alternative viewpoint on wetting of rough surfaces, underscoring heterogeneity with trapped air pockets within surface grooves. The Cassie-Baxter state, illustrated in Figure 2.8, prevents liquid droplets from infiltrating the textured surface. This results in lower sliding angles and a smaller hysteresis in the contact angle compared to the Wenzel state. The Cassie-Baxter equation is employed to quantitatively describe this behavior, considering surface fractions and contact angles on different phases. This comprehension holds significant importance in applications such as the design of superhydrophobic surfaces, where precise control of wetting properties is imperative (Kumar & Nanda, 2019).

Figure 2.8

Visual Depiction of a Composite Liquid-Vapor Interface for a Cassie-Baxter State



Compared to the Wenzel model, the Cassie-Baxter model generally features lower sliding angles and a smaller hysteresis in the contact angle. The equation governing the Cassie-Baxter model is presented below.

$$\cos\theta_{CB} = f_1\cos\theta_1 + f_2\cos\theta_2 \dots\dots\dots \text{Equation 2. 5}$$

The Cassie-Baxter equation, shown below, predicts the apparent contact angle (θ_{CB}) of a liquid droplet on a rough surface. It considers the surface fractions (f_1 and f_2) of two distinct phases (e.g., solid and air) and their respective contact angles (θ_1 and θ_2) with the liquid. Notably, for a situation involving an air-liquid interface (where phase 2 is air and its contact angle with the liquid is 180°), equation 2.5 can be simplified to equation 2.6.

$$\cos\theta_{CB} = f\cos\theta + f - 1 \dots\dots\dots \text{Equation 2. 6}$$

Within the Cassie- Baxter equation, f represents the solid surface fraction. In simpler terms, it signifies the proportion of the rough surface that is in contact with the liquid droplet (Kumar & Nanda, 2019).

Indeed, the Cassie-Baxter state can undergo a transition to the Wenzel state under specific conditions, such as when pressure is applied to the liquid droplet (Lafuma & Quéré, 2003), variations in droplet size (Reyssat et al., 2008), mechanical impact on the droplet, or subjecting the droplet to vibrations (Reyssat et al., 2006) (Bartolo et al., 2006).

In summary, this chapter offers a thorough examination of the theory of surface wettability and its significance in comprehending the interactions between liquids and solid surfaces. Grasping these concepts of surface wettability, contact angles, and their influencing factors is crucial for various applications. These include the development of superhydrophobic surfaces for oil-water separation and other functionalities.

2.4 Synthesis Techniques for Creating Superhydrophobic Surfaces

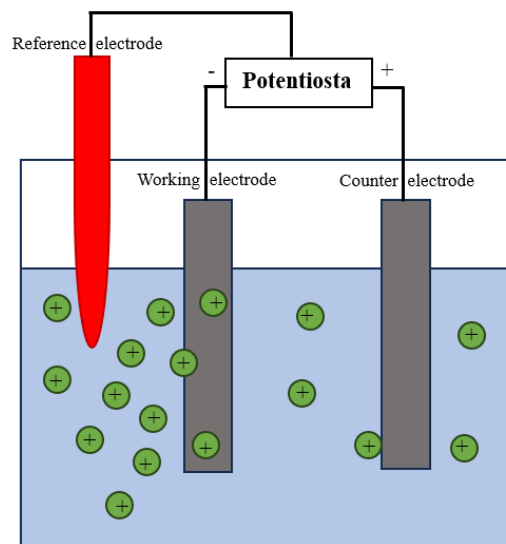
The creation of superhydrophobic surfaces encompasses a range of techniques, including dip coating, spray coating, electrochemical deposition, and more. This chapter furnishes an overview of the present advancements and obstacles encountered in the pursuit of crafting superhydrophobic surfaces.

2.4.1 Electrochemical Deposition Technique

Electrochemical deposition (Fig 2.9) offers precise control over depositing materials on tiny objects (microelectronics) at low temperatures. However, it struggles with large objects, strong materials, and perfectly controlling growth at the atomic level. So, it's great for small, precise needs but not large-scale or high-strength applications (Kumar & Nanda, 2019).

Figure 2.9

Illustration of the Electrochemical Deposition Setup



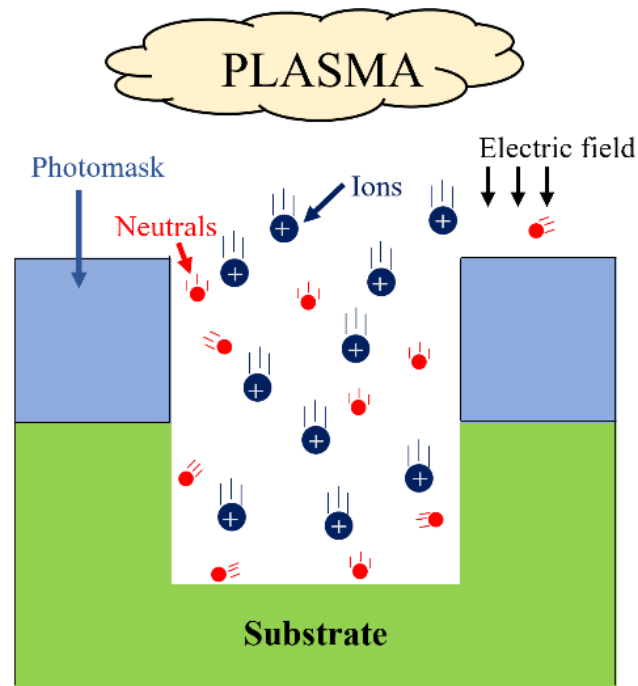
Note. Electrochemical deposition precisely builds material on a surface. Three electrodes submerged in a solution work together: one to initiate deposition (WE), another to aid electricity flow (RE), and a third to monitor for precise control (CE).

2.4.2 Plasma-Etching Technique

Plasma etching (Fig 2.10) is a fancy way of carving tiny structures on surfaces with high-speed gas. It's great for automation, material savings, and precise etching, but comes with a hefty price tag, complex controls, and potential surface damage (Kumar & Nanda, 2019).

Figure 2.10

Schematic Showing the Key Components for Plasma Etching



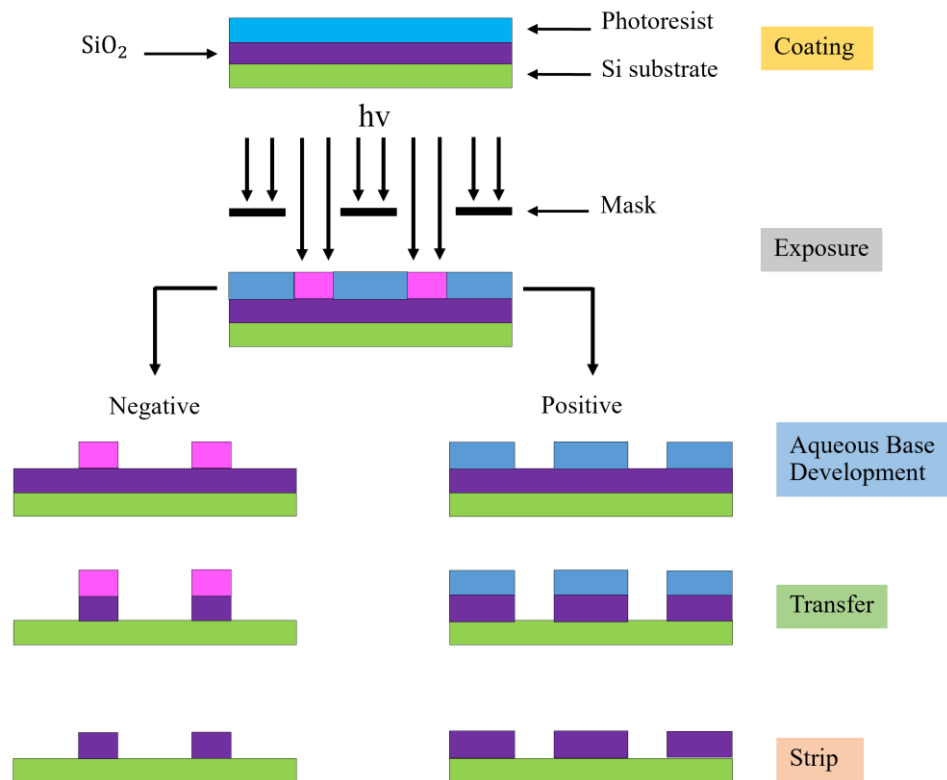
Note. This schematic depicts ions and neutral species originating from plasma. The ions, guided by the electric field, travel in a specific direction through an opening in the photomask positioned above the substrate. In contrast, the neutral species move according to a typical Maxwellian distribution, which represents a random and non-directional motion.

2.4.3 Photolithography Technique

This technique (Fig 2.11) uses light and masks to quickly create tiny circuits on chips, but it is not perfect. It can suffer from contamination and mask damage, and precisely aligning the mask can be expensive. Also, controlling the environment adds extra cost. (Kumar & Nanda, 2019).

Figure 2.11

Diagrammatic Representation of Photolithographic Patterning



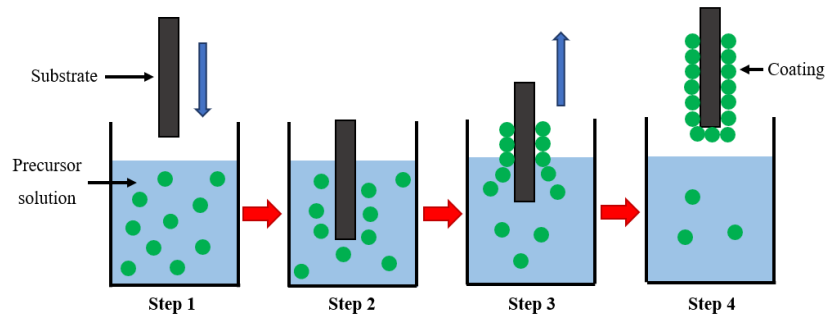
Note. There are two main types of photoresists used to create patterns with light: positive and negative. When exposed to light through a mask, negative resistance hardens in the exposed areas, while positive resistance becomes easier to dissolve. This allows either type to be used to create the desired pattern after a developer bath.

2.4.4 Dip Coating Technique

Dip coating (Fig 2.12) is a simple and fast way to get even coatings on various materials. You just dip your object and slowly pull it out, leaving a thin film. It is great for production lines and repairs, but the object needs to survive being dipped, and the coating thickness depends on how fast you pull it out. Despite these limitations, it is a valuable technique for consistent coatings (Kumar & Nanda, 2019).

Figure 2.12

Visual Depiction of the Steps Involved in Dip Coating



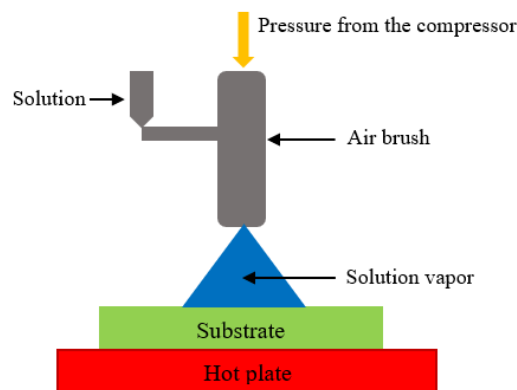
Note. Step 1) Dipping, Step 2) Drainage and Deposition, Step 3) Withdrawal and Step 4) Evaporation.

2.4.5 Spray Coating Technique

Spray coating (Fig 2.13) is a fast, cheap, and versatile way to coat large surfaces. However, it wastes material, struggles with thick coatings, and may not stick well to small objects. So, it is great for big jobs but not ideal for precise work or needing a thick layer (Kuma & Nanda, 2019).

Figure 2.13

Schematic Diagram of the Spray Coating Technique



Note. A spray jet utilizing pressure was established by employing a conventional airbrush, facilitating the production of an aerosol of the solution to be applied over the target substrate.

2.5 PDMS-Based Filter for Superhydrophobic Surface in Oil-Water Separation

The emergence of superhydrophobic surfaces has ushered in novel solutions for tackling issues associated with oil-water separation. Drawing inspiration from the lotus effect, these surfaces demonstrate remarkable water repellency, rendering them exceptionally appealing for use in applications like oil spill cleanup, wastewater treatment, and industrial separation processes. This section delves into the use of a superhydrophobic filter made from PDMS for effectively separating oil-water mixtures.

2.5.1 PDMS-Based Filter Design

To achieve efficient oil-water separation, a PDMS-based filter is designed with a superhydrophobic surface. This filter integrates superhydrophobic coatings onto a compatible substrate, like glass or plastic. The superhydrophobic nature of the filter's surface guarantees the repulsion of water while attracting and retaining oil, facilitating a clear demarcation between the two phases (Gong & He, 2020).

2.5.2 PDMS-Based Filter Design

The PDMS-based filter functions are based on the principles of superhydrophobicity and surface tension. As an oil-water mixture traverses the filter, the superhydrophobic surface repels water, causing it to form droplets that roll off the filter, while effectively capturing the oil. This behavior emulates the self-cleaning attributes observed in nature, where water droplets effortlessly cleanse contaminants from superhydrophobic surfaces (Gong & He, 2020).

2.5.3 Durability and Stability

One of the remarkable advantages of this PDMS-based filter lies in its durability and stability. This PDMS-based filter exhibits remarkable durability. It can withstand harsh conditions, such as exposure to ultraviolet radiation, peeling with tape, abrasion by sand, and contact with strong acid or base solutions, while remarkably maintaining its superhydrophobic properties. This robustness guarantees the filter's longevity and consistent performance (Gong & He, 2020).

2.5.4 Application Potential

The PDMS-based filter designed for superhydrophobic surfaces offers a versatile solution for the efficient separation of oil-water mixtures across a range of applications. This technology has widespread applications in various sectors, including environmental remediation efforts, oil spill response strategies, industrial wastewater treatment processes, and oil-water separation during manufacturing. Moreover, its adaptability to various substrates, including glass, plastic, and paper, widens its applicability to diverse engineering materials and self-cleaning glass applications. (Gong & He, 2020).

In conclusion, the fusion of superhydrophobic coatings with PDMS-based filters presents an innovative and environmentally sustainable method for tackling the pressing issue of oil-water separation. This technology not only leverages the distinct characteristics of superhydrophobic surfaces but also showcases remarkable durability and adaptability, positioning it as a promising solution for a diverse array of real-world situations demanding effective oil-water separation.

2.6 Previous Research Works on Superhydrophobic Surfaces

Various research works have made significant strides in the development of superhydrophobic surfaces. Here are some notable examples:

2.6.1 Ge et al.(2014)

Researchers developed a novel one-step spray-coating method for creating transparent, superamphiphobic coatings. This technique utilizes stringed amphiphilic silica nanoparticles and an amphiphilic sol. These coatings exhibited excellent transparency and exceptional repellency towards both water and low-surface-tension oils. They also demonstrated robustness against elevated temperatures, water exposure, and abrasion. The potential of this novel technique extends to diverse fields, including building window coatings, solar panel enhancements, electronic display production, and optical equipment manufacturing (Ge et al., 2014).

2.6.2 Wu et al.(2017)

The study introduced a simple method for producing superhydrophobic surfaces by utilizing an emulsion of nanoparticles and epoxy resin, applied through conventional household painting techniques. The resultant surfaces displayed strong water repellency, featuring a contact angle of around 152° and a low sliding angle of approximately 6° . The emulsion exhibited versatility when applied to various materials and through different methods, and the resulting surfaces showcased remarkable durability against mechanical damage and challenging conditions. This approach holds significant promise for practical and scalable applications (Wu et al., 2017).

2.6.3 Li et al.(2018)

The study devised a transparent and robust superhydrophobic coating by employing epoxy resin and hydrophobic silica particles. The coated glass retained a high level of transparency at 90.3%, closely resembling bare glass. The coatings demonstrated exceptional characteristics, including superior self-cleaning abilities, remarkable mechanical strength, and high resistance to both chemical and thermal stresses. This method strikes an effective balance between transparency and durability, presenting potential utility in various industrial applications (Zhong et al., 2018).

2.6.4 Xiao Gong and Shuang He(2020)

Shuang and Xiao Gong utilizing easily obtained materials like SiO₂ NPs and PDMS, he created superhydrophobic coatings by utilizing a simple spray-coating method. These coatings showcased outstanding water-repellent characteristics, boasting a contact angle of 156.4° and a low sliding angle of less than 5° . They proved adaptable to a range of substrates, including glass, paper, and plastic, and exhibited impressive resilience when subjected to diverse challenges like UV radiation, sand abrasion, water impact, tape peeling, and exposure to strong acids or alkalis. Additionally, these superhydrophobic surfaces demonstrated effectiveness in antifouling and self-cleaning applications (Gong & He, 2020).

Despite considerable advancements in the field of superhydrophobic surfaces, the techniques employed for their fabrication often tend to be intricate. Many of these methods necessitate specific environmental conditions or the use of costly equipment, thereby restricting their practical application.

2.7 Chapter Summary

Chapter 2 delves into the fundamental principles and recent advancements in superhydrophobic surfaces, with a particular focus on their applications, especially in oil-water separation. It emphasizes the limitations of conventional methods, necessitating innovative approaches. The chapter explores surface wettability, categorizing it into superhydrophilic, hydrophilic, hydrophobic, and superhydrophobic states, providing a detailed examination of contact angles and surface energy. We clarify wetting models, such as the Cassie-Baxter state that reveals air pockets in surface grooves, the Wenzel state for rough surfaces, and Young's equation for smooth surfaces. Various synthesis techniques, ranging from electrochemical deposition to the spray coating technique, are discussed, each with its strengths and limitations.

Furthermore, the chapter introduces a PDMS-based filter designed for oil-water separation, emphasizing its durability and wide-ranging applications. The chapter culminates by showcasing previous research works in the field, signifying the progress made and underscoring the need for simplified methods to enable practical applications of superhydrophobic surfaces.

CHAPTER 3

METHODOLOGY

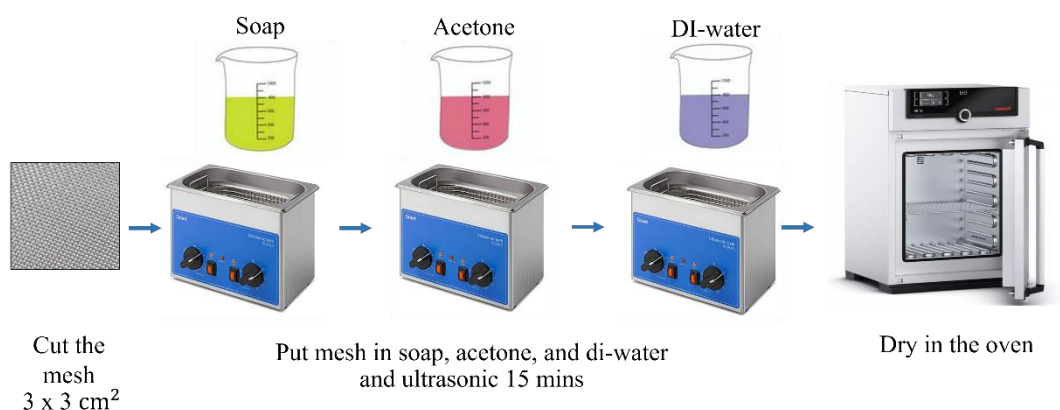
In this study, we introduce an innovative superhydrophobic PDMS-SiO₂ nanocomposite-coated mesh for efficient oil-water separation. Incorporated into a dedicated reactor, the mesh enhances the separation process. Through testing various oil-water mixtures, we evaluate the effectiveness of coating, offering valuable insights into its precision in achieving efficient oil-water separation.

3.1 Cleaning Stainless Steel Mesh

Stainless-steel mesh (SSM) is divided into 3x3cm² sections for handling convenience and cleaning. These meshes are soaked in soapy water and subjected to ultrasonication for 15 minutes to remove grease and dirt. Acetone is then used, followed by another round of ultrasonication to ensure the removal of all oily stains. After rinsing with di-water and repeating the ultrasonication, the meshes were dried in the oven, as shown in Fig 3.1. This process is repeated multiple times for thorough cleaning (Rao, 2019).

Figure 3.1

Stainless-Steel Mesh Clean Process

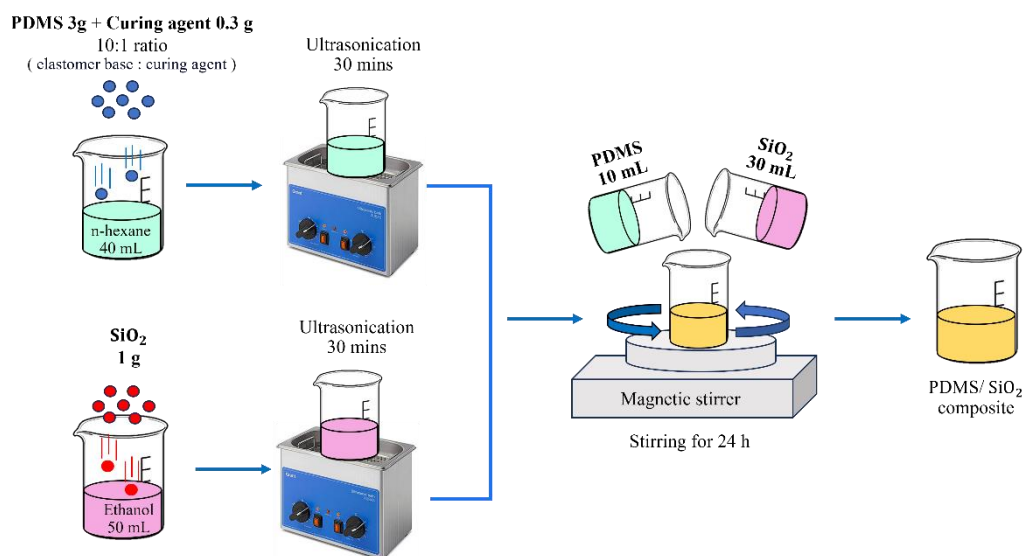


3.2 Preparation of PDMS-SiO₂ Composites

In the part of PDMS-SiO₂ composites were synthesized as follows: 3 g of PDMS base and 0.3 g of curing agent (10:1 ratio) were added in 40 ml of n-hexane and sonicated for 30 minutes (Sales et al., 2021). Separately, 1 g of SiO₂ (SiO₂, 95.9+wt%, 20-30 nm, amorphous, coated with 3-4wt% KH570-Silane Coupling Agent) was dispersed in ethanol (Han et al., 2017) and sonicated for 30 minutes. Then, 10 ml of PDMS-hexane mixture was combined with 30 ml of SiO₂-ethanol dispersion and mechanically stirred for 24 hours to achieve a uniform mixture, as shown in Fig 3.2.

Figure 3.2

PDMS-SiO₂ Composites Preparation

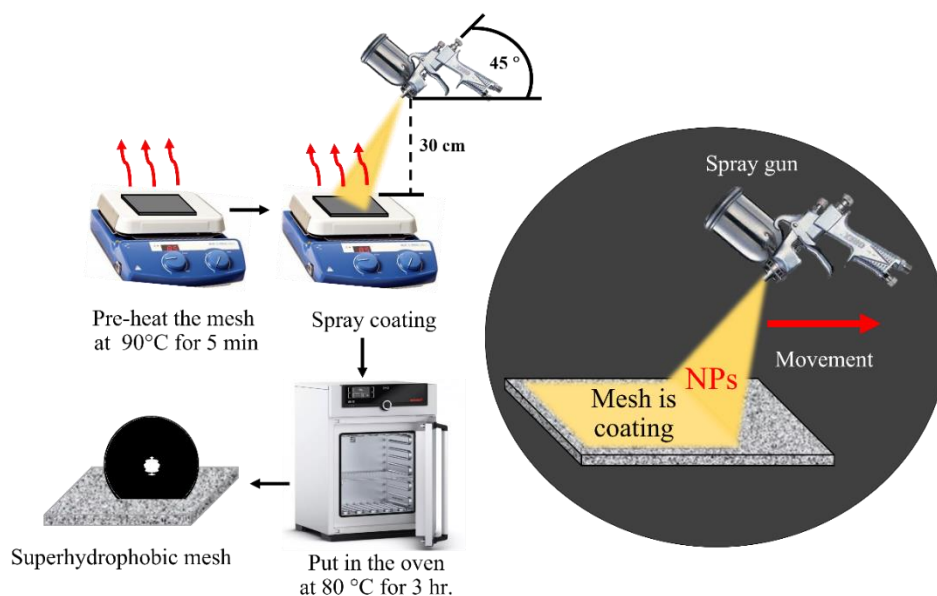


3.3 Preparation of Superhydrophobic Mesh on the Substrate Mesh by Spray Coating

For coating the SSM in this study, we use spray coating method because this method is uniform coatings on diverse materials, high production throughput, simple method, low cost, and ease of repair. The procedure involved applying the solution onto the horizontally positioned stainless-steel mesh using a pressurized spray gun connected to a compressor. In this work, the amount of substance sprayed will be small, medium, and large, which we will test with volumes of 0.5, 1.0, and 1.5 ml, respectively.

Figure 3.3

Spray Coating Technique for the Superhydrophobic Mesh Fabrication



The spray coating method is a process that requires several careful steps, as shown in Fig 3.3. First, the SSM sample was pre-heated at 90°C for 5 minutes to promote good adhesion of the spray coating. The spraying gun was moved from left to right at a constant speed by spraying slowly so that the substance was sprayed evenly and efficiently. After that, the substrate was placed in an oven at 80 °C for 3 hours to complete the curing treatment (Shen et al., 2021). Finally, the samples were stored and their surface wetting behavior was investigated.

3.4 Characterization of the Superhydrophobic Mesh

3.4.1 Scanning Electron Microscope

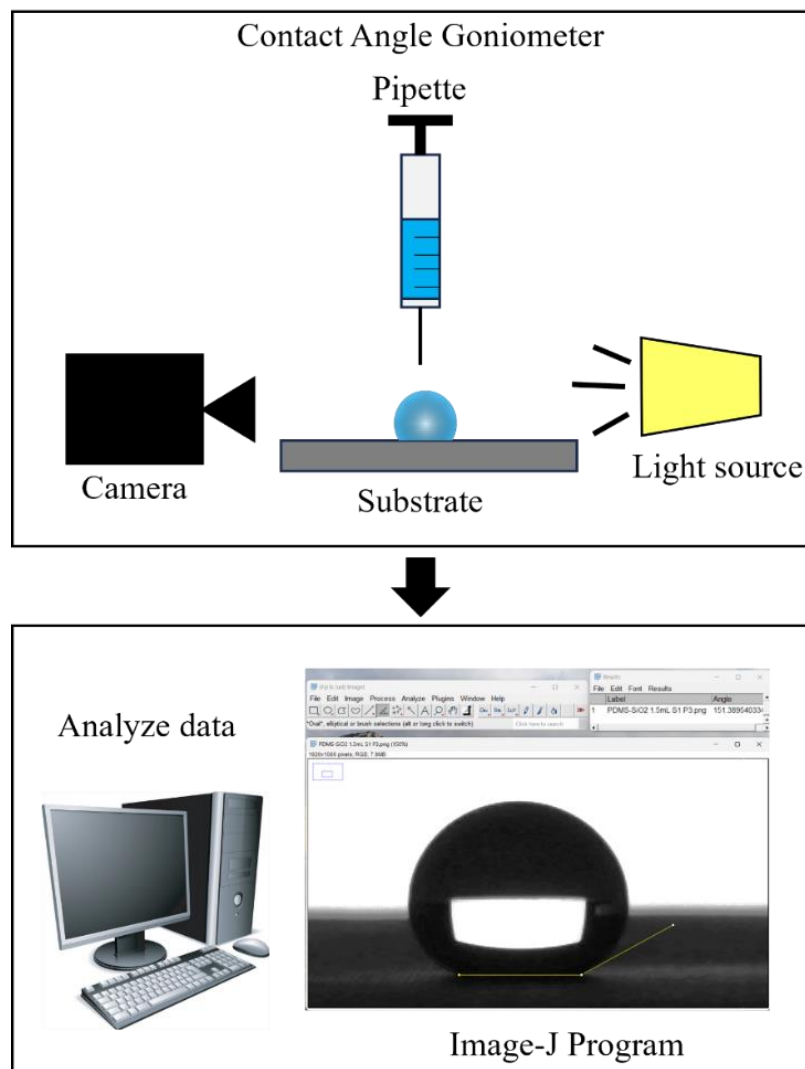
A scanning electron microscope (SEM, JEOL JSM-7800F) was used to examine the surface morphologies of coated and uncoated meshes. This machine provides information on the roughness of substrate, which provides information on the shape of nanoparticles after coating of PDMS-SiO₂ nanocomposite on the SSM.

3.4.2 Contact Angle Measurement

The contact angle (CA) measurements were performed at room temperature using a contact angle goniometer (Ossila model). A 2 μl water droplet was deposited onto the mesh surface at nine distinct locations to capture representative data. The Ossila goniometer captured a digital image of each droplet. Subsequently, image-J software, specifically its "measurement angle" function, was used to analyze these images and determine the average contact angle (WCA) as shown in Figure 3.4. This approach leverages image-J's capabilities to quantify the contact angle based on the droplet's shape within the captured image.

Figure 3.4

Contact Angle Measurement Process



3.4.3 Sliding Angle Measurement

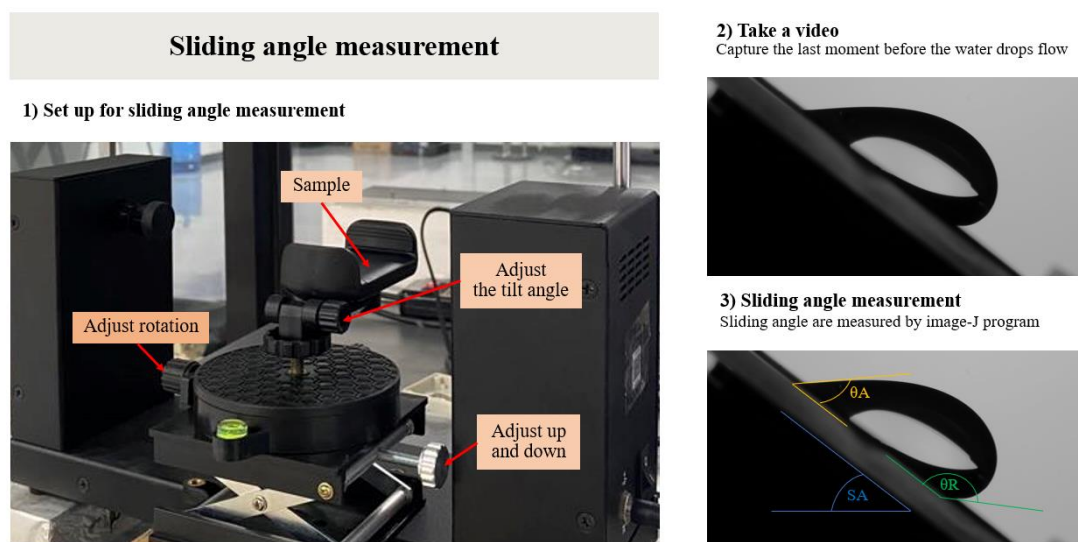
Sliding angle measurement is a technique used to assess the hydrophobicity or wetting behavior of a surface. Its definition is the smallest angle at which a droplet of liquid put on a surface will begin to glide downward. In other words, it quantifies how easily a liquid can move across a surface.

Figure 3.5 illustrates a typical sliding angle measurement device. It consists of a sample stand that can be adjusted up and down, tilted, and rotated. After placing a liquid droplet on the sample, the stand is gradually tilted until the droplet begins to move. The angle at which this occurs is recorded as a sliding angle.

The process described involves capturing a video of the droplet as the stand is tilted, and then using image analysis software (such as Image-j) to measure the contact angle of the droplet at the moment it starts to slide, as shown in Fig 3.5. The angle formed between the liquid droplet and the surface is known as the contact angle, and it is influenced by both the liquid's surface tension and the solid's surface energy.

Figure 3.5

Experiment Setup for Sliding Angle Measurement



There are two main types of contact angles that are measured in sliding angle experiments, advancing contact angle (θ_A), when the liquid is spreading on the surface. Another is receding contact angle (θ_R), when the liquid is shrinking on the surface, as shown in Fig 3.5. The contact angle hysteresis is the difference between the advancing and retreating contact angles. This hysteresis, which is correlated with surface heterogeneity and roughness, is a gauge of the wetting process' reversibility.

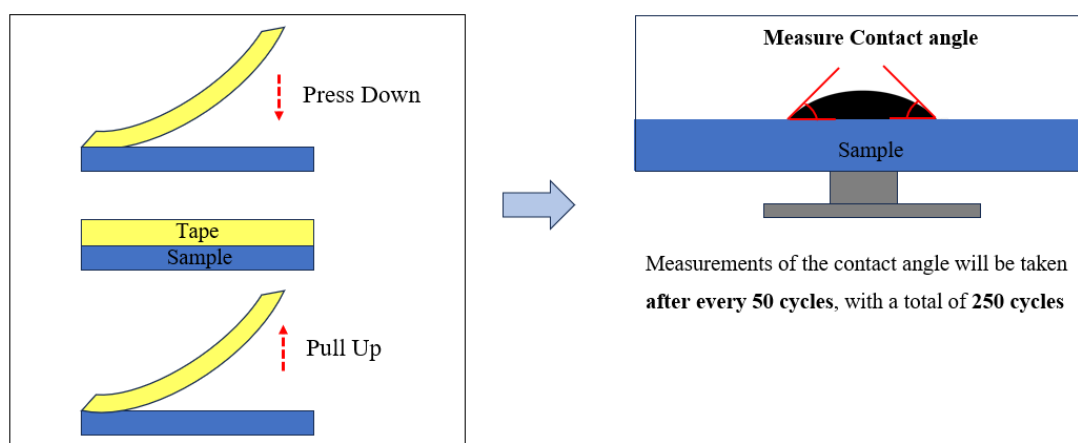
Sliding angle measurement is a flexible method that may be applied to the study of many different surfaces, including artificial and biological materials. It is an invaluable resource for comprehending the features of a material's surface and for creating new materials with the appropriate wetting qualities.

3.5 Durability Test

To investigate the durability of the prepared superhydrophobic coatings, the tape peeling method will be employed. This will entail recording the WCA to confirm the continued superhydrophobic properties of coating. Additionally, a tape peeling test using regular adhesive tape was conducted to assess the adhesion between the superhydrophobic coating and the substrate. Measurements of the WCA will be taken after every 50 cycles, with a total of 250 cycles in the study (Gong & He, 2020), as shown in Fig 3.6.

Figure 3.6

Durability Testing of the Mesh



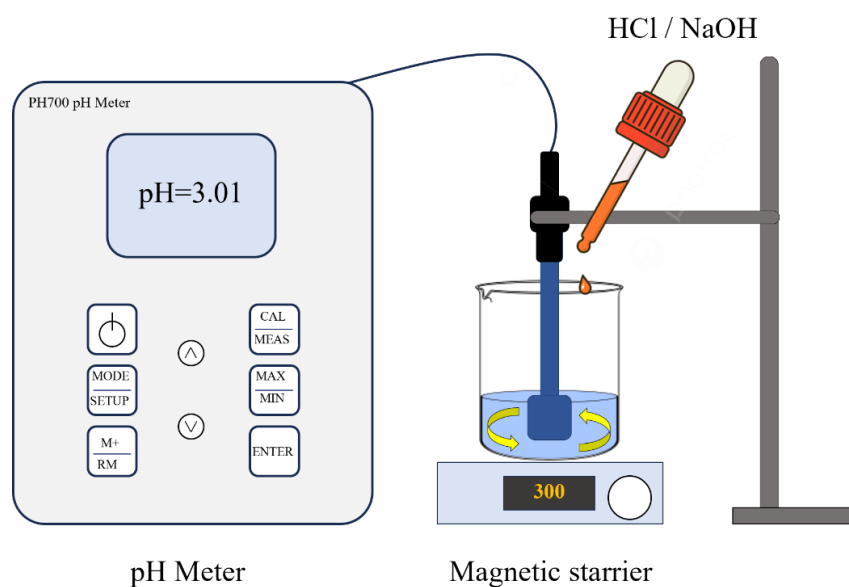
3.6 Chemical Stability Test

This section details the preparation of water solutions with varying pH values and the subsequent measurement of WCAs on the fabricated meshes.

The pH range of the aqueous solutions was 3 (acidic) to 13 (base). To achieve this, hydrochloric acid (HCl) and sodium hydroxide (NaOH) were used for acidic and basic solutions, respectively. Prior to use, the pH meter was calibrated to ensure accurate measurements. The acid or base was then added dropwise (0.1 mol concentration) into deionized water using a magnetic stirrer to ensure thorough mixing, as shown in Fig 3.7. The addition continued until the desired pH value was reached, as measured by the calibrated pH meter. Three replicates were performed for each pH level to ensure measurement accuracy.

Figure 3.7

Preparation of Water with a pH of 3-13 by Using Hydrochloric Acid and Sodium Hydroxide



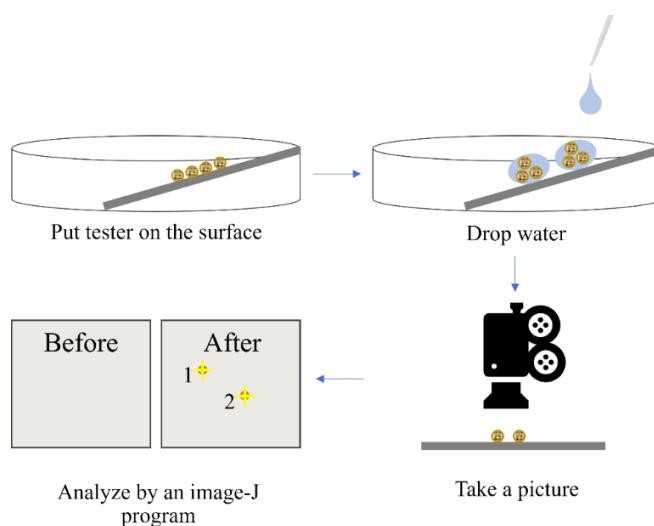
The WCAs of all seven samples (uncoated mesh, pure PDMS-coated meshes with three volumes (0.5, 1.0, and 1.5ml), and PDMS-SiO₂ coated meshes with the same three volumes) were measured using a CA goniometer. A water droplet of a defined volume (2μl) was dispensed onto the mesh surface using a micro-syringe. The instrument captured a digital image of the droplet profile on the surface, and the software calculated the WCA based on the interfacial angles. The WCA measurements were repeated at least three times for each sample at each pH level to account for any potential variations. The average WCA was then calculated to represent the water repellency of each sample under different pH conditions.

3.7 Self-Cleaning Ability Test

To demonstrate the self-cleaning capability of the fabricated superhydrophobic mesh, we tested our mesh's self-cleaning ability with sand, soil, dust, and graphite. First, the fabricated mesh is exposed to these contaminants. Then, the mesh is tilted in a dish and water is added, simulating a rinsing process. High-resolution images of the mesh surface are captured with a Dino-Lite microscope both before and after this water rinse. Finally, Image-J software is used to analyze these images, quantifying the amount of contaminant remaining on the mesh surface. By comparing the pre- and post-rinse data, we can assess the cleaning effectiveness of the superhydrophobic mesh based on the reduction of contaminants after the water rinse, as shown in Fig 3.8 below. This approach leverages the water-repelling properties of the superhydrophobic mesh, where water carries away contaminants during the rinsing stage (Gong & He, 2020).

Figure 3.8

Self-Cleaning Ability Testing of the Mesh



3.8 Oil-Water Separation Apparatus Fabrication

This reactor integrates a tilted stainless-steel mesh (SSM) within a designated slot. The positioning of the separation reactor was determined based on the concept of the sliding angle. To calculate this angle, experiments were conducted by placing water droplets on both coated and uncoated sections of the SSM. The substrate was tilted, and the critical angle for droplet sliding was measured.

Figure 3.9

Schematic Showing the Components Involved in the Oil-Water Separation Process

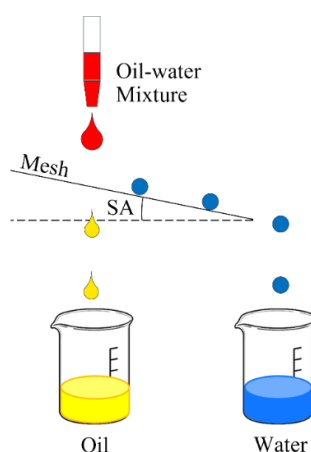


Figure 3.9 illustrates an experimental arrangement designed for oil-water separation. The top section functions as the inlet for the mixture, which subsequently passes through a coated stainless-steel mesh (SSM) within the reactor. In this process, the oil separates and gathers in a lower container, while the water descends along a slanted mesh and is collected independently. This configuration showcases an efficient approach to oil-water separation, highlighting the critical role of the coated mesh.

3.9 Efficiency of Oil-Water Separation

Efficiency in oil-water separation stands as a crucial metric for evaluating the effectiveness of separation techniques. This parameter holds pivotal importance. This section delves into the methodologies and metrics employed to quantify the success of these processes.

In this study, various types of oils including cooking oil, diesel B7, gasohol 95, mineral oil, hexane, and toluene, were blended with water to form mixtures. To facilitate the efficient separation of oil from water, a specially designed superhydrophobic PDMS-SiO₂ nanocomposite coated mesh was securely placed within a dedicated separation reactor. The mixtures, consisting of a 1:4 v/v ratio of oil to water, totaling 5 ml. Throughout the separation process, gravity played a pivotal role as the primary driving force, as shown in Fig 3.10.

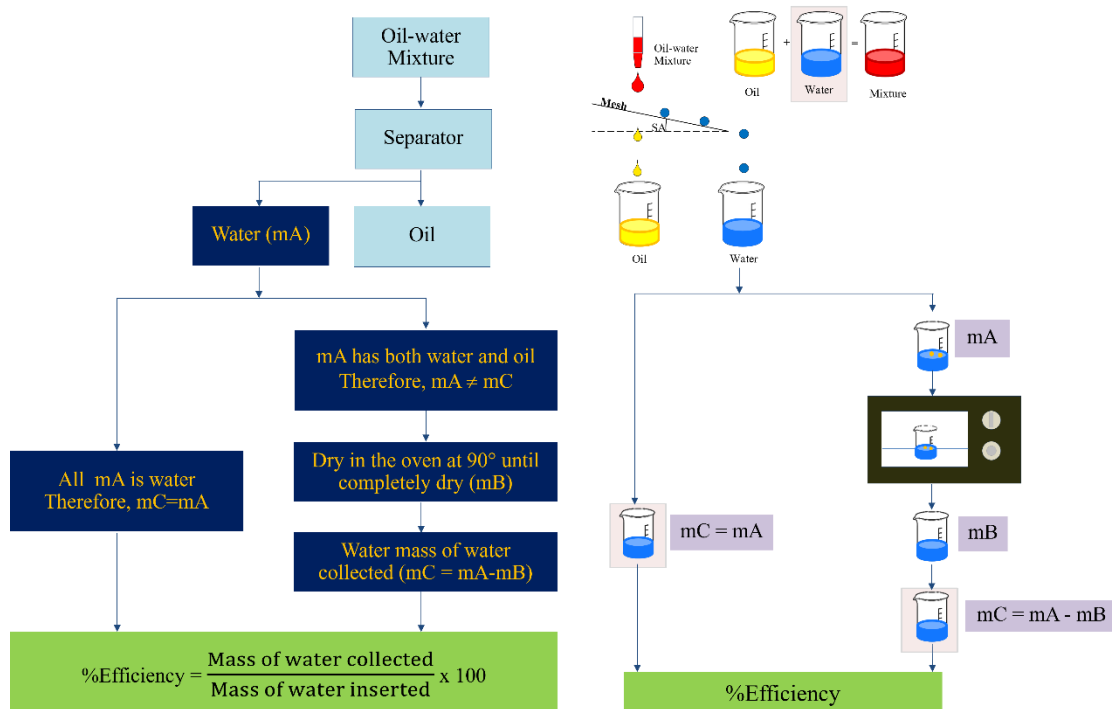
The process outlined in the diagram (Fig 3.10) quantifies the effectiveness of a filter in separating oil from water. The oil-water mixture is first passed through the filter, and the collected water is weighed (m_A). If no visible oil contamination is present in the collected water (m_A), it is assumed to be pure water. In this case, the mass of collected water (m_A) is directly assigned the value of m_C (mass of pure collected water). The efficiency (EFF) of the separation process can then be calculated as a percentage using this value.

However, if oil is visible in the collected water (m_A), further steps are required. The water sample (m_A) must be thoroughly dried in an oven to remove any water contamination. Once completely dry, the water is weighed again (m_B). The mass of pure collected water (m_C) is then determined by subtracting the initial weight (m_A)

from the weight after drying (m_B). This effectively removes the contribution of the oil's mass to the weight measurement. Finally, the efficiency (EFF) of the oil-water separation is calculated as a percentage. It represents the ratio of the mass of pure collected water (m_C) to the initial mass of water in the mixture.

Figure 3.10

The Process of Water and Oil Filtration



Note. m_A is mass of water after separated by filter, m_B is mass of water after dry in the oven, and m_C is mass of water collected.

To evaluate how well this separation works, we calculate a ratio. This ratio compares the amount of water collected after the separation process to the initial amount of water put in. The equation below shows how this calculation is done (Li et al., 2015).

$$\% \text{ Efficiency} = \frac{\text{Mass of water collected}}{\text{mass of water inserted}} \times 100 \dots\dots\dots \text{Equation 3.1}$$

CHAPTER 4

RESULTS AND DISCUSSIONS

This chapter explains the performance of coated meshes, and the characterization of the samples. PDMS-SiO₂ coatings displayed exceptional durability, chemical stability, and self-cleaning properties. Efficiency tests revealed their effectiveness in oil-water separation, with the optimal coating volume depending on the oil type. These results highlight the potential of PDMS-SiO₂ meshes for various applications.

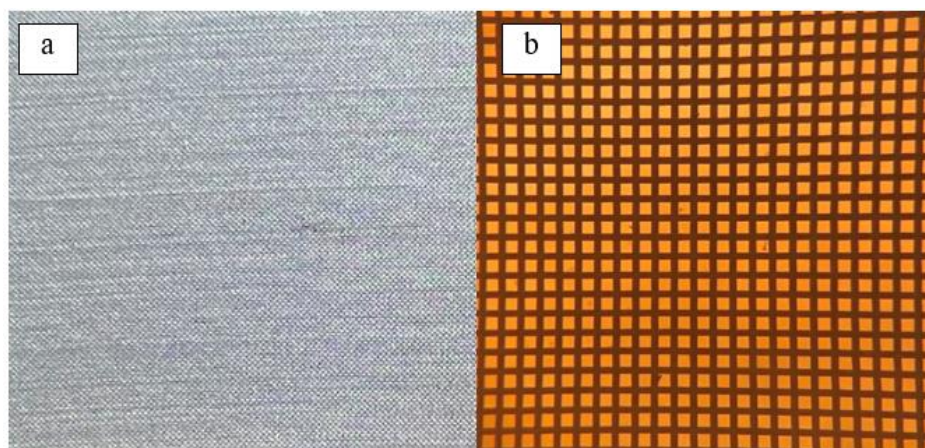
4.1 Stainless-Steel Mesh Measurement

The dimensions of the perforations in the stainless-steel mesh were meticulously assessed using an optical microscope and images from multiple locations were analyzed with the help of a program called ImageJ. Subsequently, these measurements were aggregated to yield an average value. Figure 4.1 presents a visual representation of the stainless-steel mesh (Stainless 304, 200 mesh), comparing images captured by a camera (left) and by a microscope at 40x magnification (right). The mesh aperture was estimated from the microscopic image which yielded a mean value of 75.6 μm . This value corroborated well with the technical specification of the stainless-steel mesh which indicated the mesh aperture as 75 μm .

Figure 4.1 presents a visual representation of the SSM, comparing images captured from both the camera (left) and the microscope at 4x magnification (right). The images corroborate our quantitative findings, providing a comprehensive view of the mesh structure. Notably, the microscopic image highlights the finer details, showcasing the precision achieved in our measurements. This convergence of quantitative and visual data reinforces the reliability of our results, affirming that the stainless-steel mesh closely adheres to the specified dimensions.

Figure 4.1

Stainless 304 Wire Mesh Filter 200 Mesh- 75 Micron



Note. a) Image of stainless-steel mesh captured using a camera (left) and b) captured under a microscope (right).

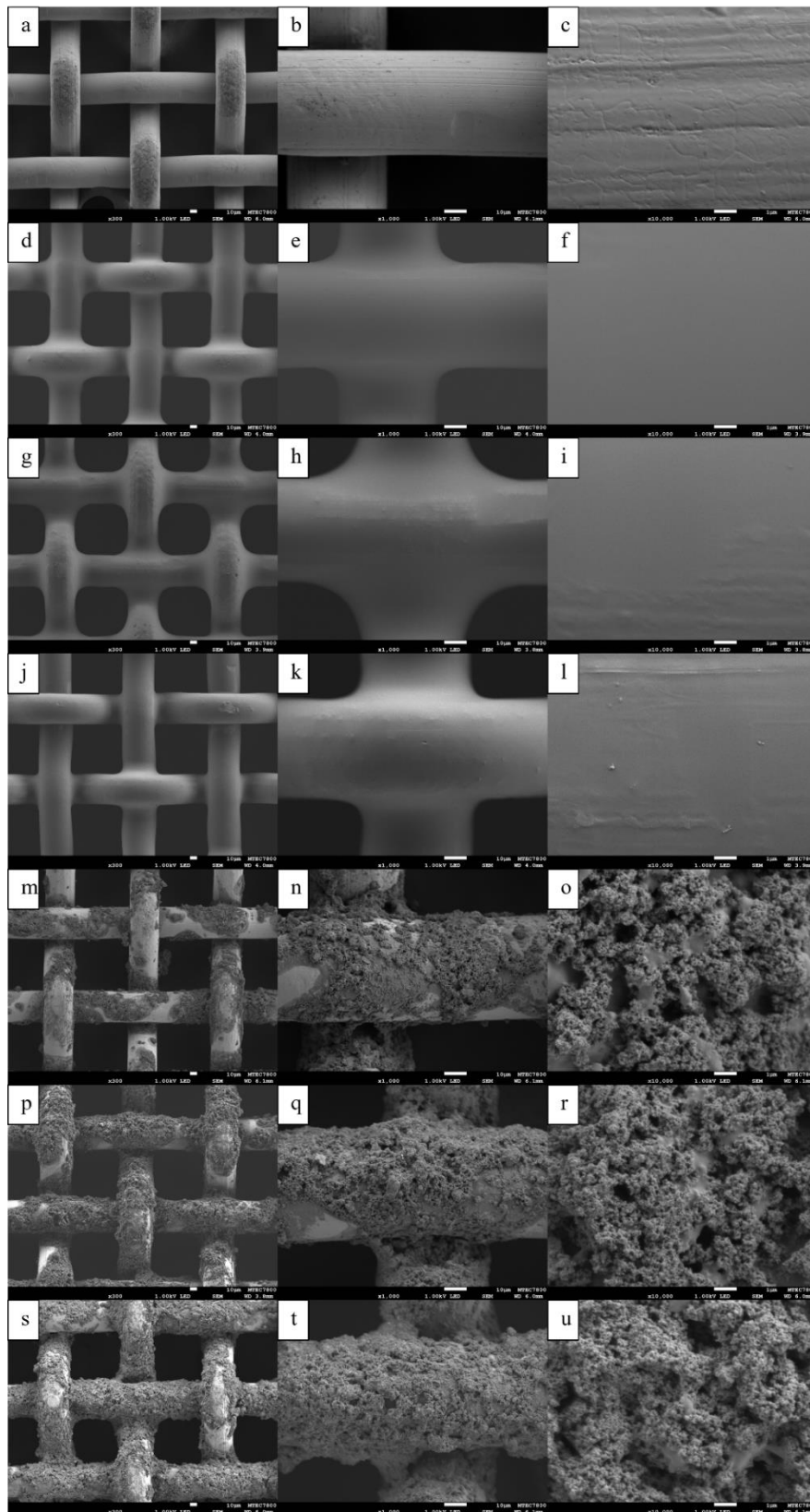
4.2 Surface Morphology

The surface morphologies of uncoated and coated meshes were observed under scanning electron microscope (SEM), and the SEM micrographs of various samples are shown in Figure 4.2 below.

SEM revealed distinct surface morphologies for the uncoated, pure PDMS coated, and PDMS-SiO₂ coated meshes, with variations observed within each type based on coating volume. Figure 4.2 (a)-(c) shows the SEM of the uncoated mesh at 300x to 10,000x magnifications respectively, where the stainless-steel wire surface with little roughness is clearly visible. Upon coating with pure PDMS (Figure 4.2 (d)-(l)), a smoother coating on the stainless-steel wire was observed. Amount of PDMS sprayed was varied as 0.5, 1.0 and 1.5 ml to see the effect on the surface coating. It should be noted that compared to the uncoated surface, pure PDMS coated surfaces exhibited smoother surfaces irrespective of the amount of PDMS sprayed.

Figure 4.2

SEM Micrographs of Uncoated and Coated Mesh



Note. Image (a), (b), and (c) represent uncoated mesh at 300x, 1000x, and 10000x magnification respectively. Image (d), (e), and (f) represent 0.5 ml pure PDMS coated mesh at 300x, 1000x, and 10000x magnification respectively. Image (g), (h), and (i) represent 1.0 ml pure PDMS coated mesh at 300x, 1000x, and 10000x magnification respectively. Image (j), (k), and (l) represent 1.5 ml pure PDMS coated mesh at 300x, 1000x, and 10000x magnification respectively. Image (m), (n), and (o) represent 0.5 ml PDMS-SiO₂ coated mesh at 300x, 1000x, and 10000x magnification respectively. Image (p), (q), and (r) represent 1.0 ml PDMS-SiO₂ coated mesh at 300x, 1000x, and 10000x magnification respectively. Image (s), (t), and (u) represent 1.5 ml PDMS-SiO₂ coated mesh at 300x, 1000x, and 10000x magnification respectively.

In contrast, a significantly rough surface coating was observed when PDMS-SiO₂ was coated on the stainless-steel surface, as shown in Figure 4.2 (m)-(u). At 0.5 ml, the PDMS-SiO₂ coating showed partial coverage on the stainless-steel surface. At 1.0 ml, the coverage was improved and at 1.5 ml complete coverage was observed. High magnification SEM images revealed that unlike the pure PDMS, the PDMS-SiO₂ coatings are uneven, rough, and porous in nature.

The observed morphological differences of uncoated, pure PDMS and PDMS-SiO₂ coatings can be attributed to the presence of SiO₂ nanoparticles. The nanoparticles likely disrupt the smooth, uniform structure of pure PDMS, introducing roughness and texture through their integration within the matrix. This is evident in the increased surface features observed in the PDMS-SiO₂ images compared to their pure PDMS counterparts at all coating volumes.

Furthermore, the variation in morphology across different coating volumes within each type suggests a potential influence of coating thickness on the deposition and distribution of material. Thicker coatings (1.0 ml and 1.5 ml) tend to exhibit more pronounced wrinkles, folds, and even cracks, possibly due to challenges in achieving uniform coverage and potential stress build-up within the thicker layers.

The presence of agglomerated nanoparticles in the 1.5 ml PDMS-SiO₂ coating is another noteworthy finding. Although this might introduce some non-uniformity, it could also contribute to enhanced surface roughness, potentially favoring hydrophobicity by reducing solid-liquid interaction area, thus promoting water droplet rolling.

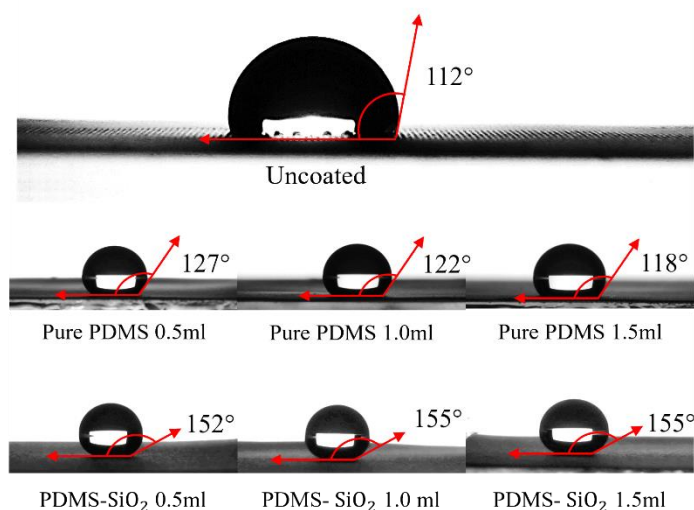
In conclusion, the SEM images unveil distinct morphological differences between pure PDMS and PDMS-SiO₂ coatings, highlighting the impact of nanoparticle incorporation on surface texture and uniformity. These findings provide valuable insights into the potential relationship between coating morphology and hydrophobicity, suggesting avenues for further optimization through tailored nanoparticle distribution and controlled coating thickness.

4.3 Surface Wetting Behavior

In order to evaluate the surface wetting behavior of the various coated and uncoated surfaces, we have carried out a water contact angle (WCA) measurement on the sample surface, as explained in detail in the previous chapter. Figure 4.3 shows the images of water droplet sitting on the sample surfaces, Uncoated stainless-steel samples displayed a hydrophobic surface with WCA of 112°. Pure PDMS coatings offered minimal influence, changing the WCA to 127°, 122°, and 118° for the 0.5 ml, 1.0 ml, and 1.5 ml samples respectively. In contrast, PDMS-SiO₂ coatings exhibited superhydrophobic nature with significantly increased WCA of 152°, 155°, and 155° for the 0.5 ml, 1.0 ml, and 1.5 ml PDMS-SiO₂ samples respectively.

Figure 4.3

Images Showing Water Droplet Sitting on the Coated and Uncoated Stainless-Steel Surfaces



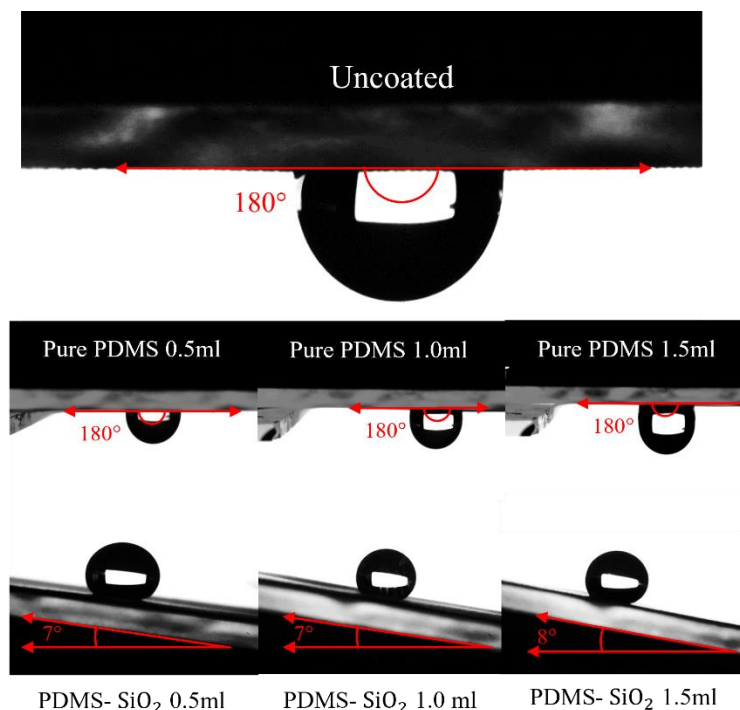
Uncoated and Pure PDMS coated mesh displayed similar wetting behavior with WCA around 120°, which is mainly due to their similar and smoother surfaces as can be observed in Figure 4.3. PDMS-SiO₂ coated mesh, on the other hand, achieved significantly higher water contact angles (around 155°), indicating a superhydrophobic water-repellent surface due to the enhanced roughness of the coated layers, as observed in figure 4.3. The porous and rough surface creates air pockets at the surface minimizing the water and solid surface interaction promoting the hydrophobicity of the surface.

In order to further evaluate the dynamic surface wetting behavior, we investigated the sliding angle of the various coated and uncoated samples, as shown in figure 4.4 below. Interestingly, uncoated, and pure PDMS-coated samples (at all volumes) did not display any sliding angle, and the water droplet was observed to remain on the surface maintaining its shape when the samples were rotated 180° indicating a Wenzel-type homogenous wetting surface. Conversely, all the PDMS-SiO₂ coatings exhibited a very low sliding angle of around 7°, demonstrating Cassie-Baxter type heterogenous wetting nature suitable for superhydrophobic and self-cleaning applications. The contact angle hysteresis measured for these samples demonstrated a value of around 20° suggesting a

transition to a more mobile wetting state due to the Cassie-Baxter state with trapped air pockets reducing liquid contact area to solid.

Figure 4.4

The Image Shows the Sliding Angle of Each Surface



4.4 Evaluation of Oleophilic Behavior

The oleophilic behavior of the coated and uncoated mesh samples was studied to assess the influence of the fabricated coatings on oil repellency and potential flow behavior. Six different oils, including Gasohol, Diesel, Mineral oil, Cooking oil, Hexane, and Toluene, were used for this evaluation. Oil contact angle (OCA) was measured for seven samples: uncoated mesh, pure PDMS-coated meshes with three volumes (0.5, 1.0, and 1.5 ml), and PDMS-SiO₂ coated meshes with the same three volumes as shown in Fig 4.5.

Figure 4.5

Images of Oil Contact Angle Measurements with Different of Oils

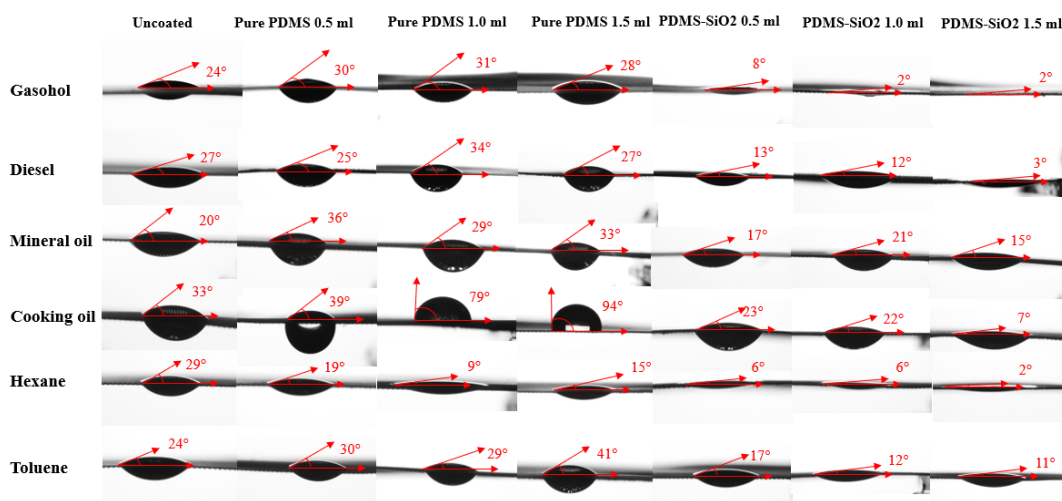
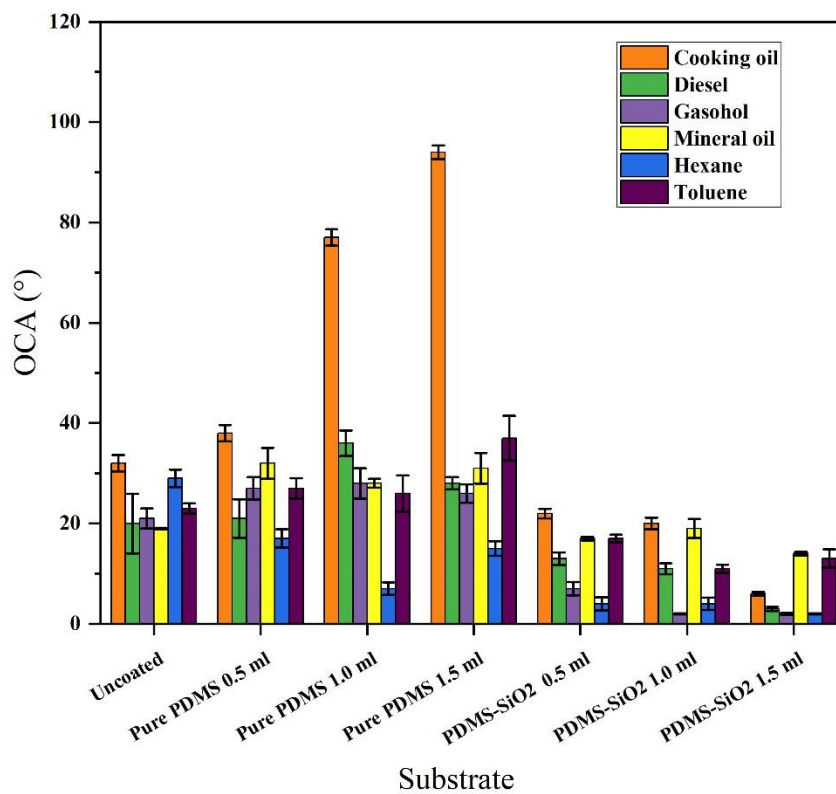


Figure 4.6

Variations in Oil Contact Angles on Uncoated and Coated Stainless-Steel Mesh



The results (presented in Fig 4.6) reveal a clear trend in oil repellency based on surface modification. Uncoated meshes exhibited relatively low OCA values (ranging from $\sim 20^\circ$ to 33°), indicating an oleophilic surface. This suggests that oil readily spreads on the uncoated stainless-steel surface, potentially allowing oils to flow through it.

In contrast, introduction of PDMS coatings (pure PDMS) resulted in a moderate increase in OCA values for most of the oils, except for the cooking oil where a significant increase in the OCA from 32° to 94° was observed. Overall, it was observed that pure PDMS coating tend to increase the oleophobicity of the surface compared to the uncoated surfaces. However, the observed OCAs with pure PDMS remained relatively low (below 40°), allowing oil samples to partially flow through the mesh similar to the uncoated mesh.

Significantly reduction in the OCA was observed in case of the PDMS-SiO₂ coated mesh samples. All PDMS-SiO₂ samples (regardless of coating volume) demonstrated substantially lower OCA values for all oil types, ranging between 2° (Gasohol, Diesel, and Hexane) to 22° (Cooking oil). Despite the rough surface texture introduced by nano-silica particles in PDMS-SiO₂ coatings, these coatings exhibit strong oleophilic nature due to the low surface energy of the coating. The low surface energy is mainly introduced by the hydrophobic nature of the silane functionalized SiO₂ particles, allowing oil to flow more readily through it compared to the uncoated samples.

The observed variation in OCA values depending on the oil type (e.g., higher for cooking oil, lower for hexane) could be due to differences in their surface tension and viscosity. Less viscous and lower surface tension oils can spread easily on the surface, leading to small OCA compared to more viscous or higher surface tension oils.

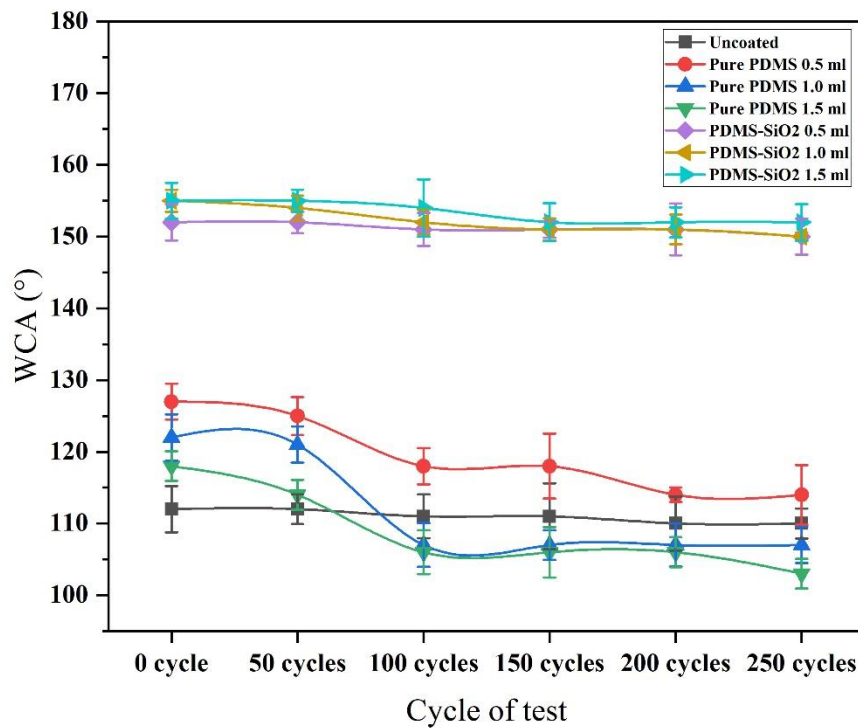
4.5 Durability Test

The durability of the coated stainless-steel mesh was tested using a tape-test method, as described in the previous chapter. Briefly, a tape was repeatedly attached to the coated surface and removed up to 250 times, and changes in the WCA was monitored in every 50 cycles of adhesion and removal. The variations in the WCA during this tape test for different coated and uncoated samples are shown Fig 4.7 below. In case of the uncoated

samples, the WCA remained nearly the same varying between 112° to 110°. While pure PDMS coatings, regardless of the volume sprayed (0.5, 1.0, and 1.5 ml), experienced a noticeable decline in WCA of 10-12% during the tape tests. For the 0.5 ml pure PDMS coating the WCA was observed to drop from 127° to 114° (~10% reduction), while 1.0 ml and 1.5 ml pure PDMS coatings resulted WCA drop from 122° to 107° (~12% reduction) and 118° to 106° (~10% reduction), respectively. This indicates that the pure PDMS coatings are not very stable and getting removed during the peeling of the tape resulting in WCA similar to the uncoated samples after about 150 cycles.

Figure 4.7

Changes in Water Repellency of the Mesh Observed after a Durability Test



On the other hand, PDMS-SiO₂ coatings demonstrated remarkable stability throughout the test, maintaining consistently high WCA values (>150°) with minimal change, as shown in Fig 4.7. This exceptional performance is attributed to the robust and cross-linked structure created by the incorporated nanoparticles, further enhanced by strong

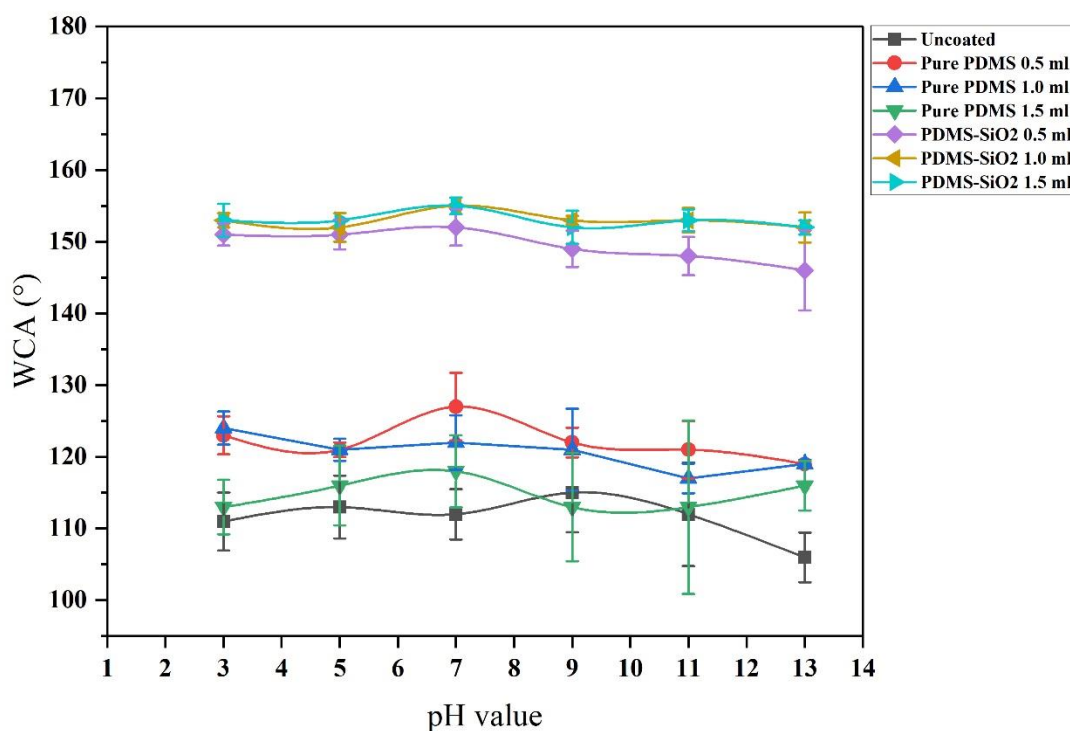
adhesion between silane modified SiO₂ nanoparticles and PDMS chains. These findings clearly demonstrate the superior durability of PDMS-SiO₂ coatings, making them highly suitable for applications requiring sustained hydrophobicity and superhydrophobicity under demanding mechanical stress.

4.6 pH stability Test

We then investigated the influence of water pH on the WCA of uncoated and coated meshes. The WCA measurements were conducted on seven samples: uncoated, PDMS coated with three different volumes (0.5, 1.0, and 1.5 ml), and PDMS-SiO₂ coated with the same three volumes. The pH of the water used for the measurements ranged from 3 (acidic) to 13 (base), encompassing a broad spectrum.

Figure 4.8

Influence of Solution Acidity (pH 3-13) on the Wettability of Different Samples as Measured by Water Contact Angle



The results, presented in Fig 4.8 , reveal a minimal effect of water pH on the WCA for most of the samples. Uncoated and pure PDMS-coated meshes exhibited consistent WCAs across the entire pH range, with values ranging from approximately 106° to 124°. This suggests that the inherent hydrophobicity of these surfaces is relatively unaffected by changes in water acidity or alkalinity.

In contrast, PDMS-SiO₂ coatings displayed a more intriguing behavior. While their WCAs remained relatively high across all pH values (above 150°), there was a slight decrease observed at extremely acidic (pH = 3) and base (pH = 13) conditions compared to neutral pH (pH = 7). This subtle trend could be attributed to the interaction between the charged Si-OH groups on the nanoparticle surface and the H⁺ or OH⁻ ions present in acidic and basic solutions, respectively. Wever, further investigation would be necessary to elucidate the exact mechanisms behind this observation.

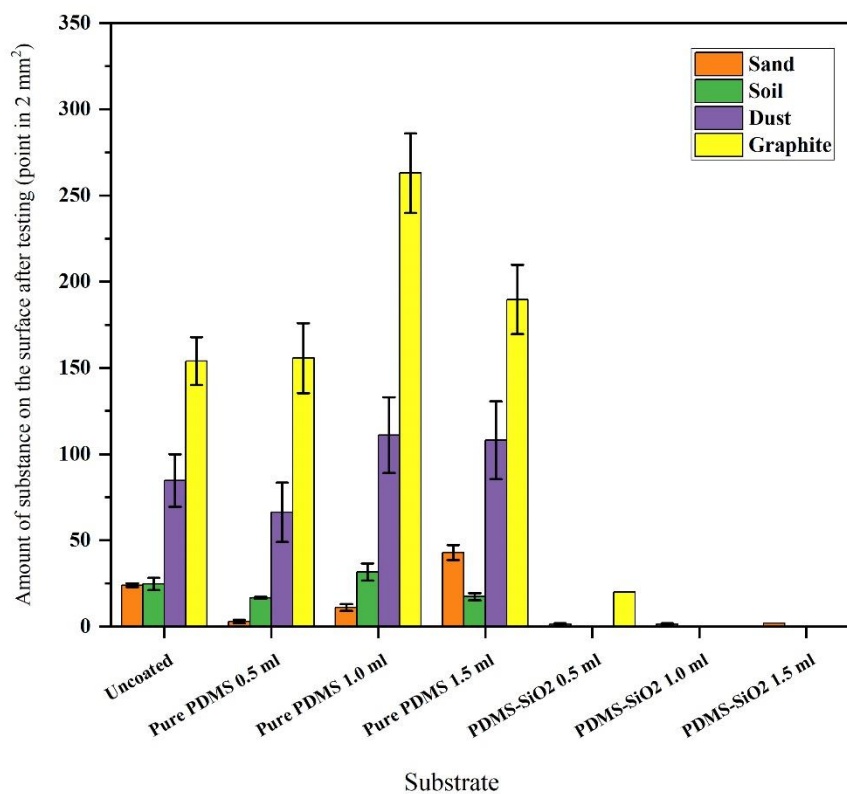
It is important to note that neutral pH (pH 7) represents the typical condition of water encountered in most applications. Here, all samples exhibited good water repellency, with PDMS-SiO₂ coatings demonstrating the highest WCAs (155°), highlighting their superior hydrophobicity. This superior performance aligns well with the expected properties of these coatings for potential applications.

4.7 Self-Cleaning Test

The self-cleaning ability of the fabricated coated and uncoated meshes was evaluated by analyzing their effectiveness in removing various contaminants upon water droplet application. Sand, soil, dust, and graphite powder were chosen as model contaminants to assess the cleaning performance across different particle sizes and types. The details of the self-cleaning test and how it was conducted are given in the previous chapter.

Figure 4.9

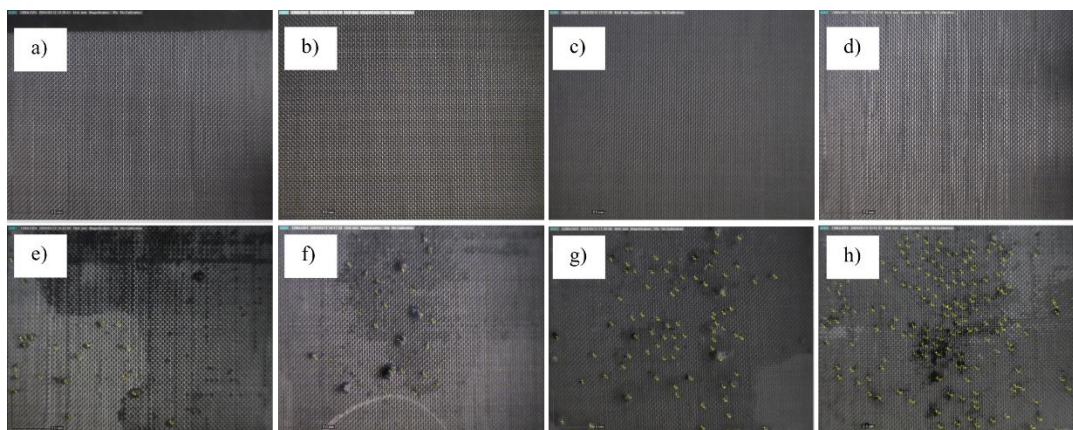
Amount of Substance on the Sample Surface after Self-Cleaning Test of Each Sample



The results (presented in Fig 4.9) demonstrate a clear distinction between the different sample types. Uncoated samples, as expected, exhibited significant residue after the self-cleaning test. The number of remaining contaminant particles ranged from 24 (sand) to 154 (graphite), indicating limited self-cleaning capability for uncoated meshes due to strong adhesion of contaminants to the surface, as shown in Fig 4.10.

Figure 4.10

Self-Cleaning Test on Uncoated Surface Mesh
















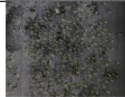







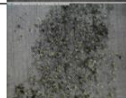


Note. Images of a) ,b) ,c), and d) are images of uncoated meshes before being tested with sand, soil, dust, and graphite, respectively. Images of e) f) g) h) are images of uncoated meshes after being tested with sand, soil, dust, and graphite, respectively.

Pure PDMS coatings showed some improvement in the case of sand and soil compared to the uncoated samples but demonstrated poor self-cleaning ability against dust and graphite powder. While not achieving complete removal, they exhibited a higher number of residual contaminants on the surface after the self-cleaning test, as shown in figure 4.11. In case of the graphite powder almost 70% higher particle count was found with pure PDMS coatings, compared to the uncoated samples, while for dust the same was almost 30% more. It should be noted that both graphite and dust particles have high surface energy and they tend to form strong physical adsorption on PDMS surface making them difficult to remove from the surface.

Figure 4.11





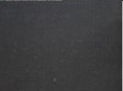



















Self-Cleaning Test on Pure PDMS Surface Mesh

Pure PDMS Substrate		Sand	Soil	Dust	Graphite
0.5 ml	Before				
	After				
1.0 ml	Before				
	After				
1.5 ml	Before				
	After				

In case of the PDMS-SiO₂ coatings remarkable self-cleaning properties are observed. Figure 4.12 below shows the surface of the PDMS-SiO₂ coated meshes before and after the self-cleaning test. After the test, no visible residue was observed on any of the PDMS-SiO₂ samples (0.5 ml, 1.0 ml, and 1.5 ml volumes) for all contaminant types (sand, soil, dust, and graphite). This exceptional cleaning performance can be attributed to the superhydrophobicity and low sliding angle of the PDMS-SiO₂ coatings, as discussed previously, mimicking the natural self-cleaning surface of the lotus leaf. These findings highlight the significant advantage of PDMS-SiO₂ coatings for applications where self-cleaning functionality is crucial. Their ability to effectively remove various contaminants underscores their potential in various applications like filtration systems, self-cleaning surfaces, and microfluidic devices.

Figure 4.12

Self-Cleaning Test on PDMS-SiO₂ Surface Mesh

PDMS – SiO ₂ Substrate		Sand	Soil	Dust	Graphite
0.5 ml	Before				
	After				
1.0 ml	Before				
	After				
1.5 ml	Before				
	After				

4.8 Oil-Water Separation Test

This section explores the effectiveness of PDMS-SiO₂ coated mesh filters in separating oil from oil-water mixture. In order to conduct the oil-water separation tests, we have constructed a custom-made apparatus, as shown below, where the PDMS-SiO₂ coated mesh filter was placed at an angle slightly higher than their sliding angle (7°) and oil-water mixture was poured on it which were then collected separately in two separate beakers placed below the mesh filter. The details of the apparatus construction in given in the previous chapter. A consistent volume of 4 g of water was used as the starting material in each separation experiment, to which different quantities of six types of oil was added to evaluate the separation efficiency of the fabricated system. The separation efficiency was evaluated by measuring the amount of water recovered after filtration and then dividing it by the initial amount of water added for filtration.

Figure 4.13

Experiment Setup for Oil-Water Separation

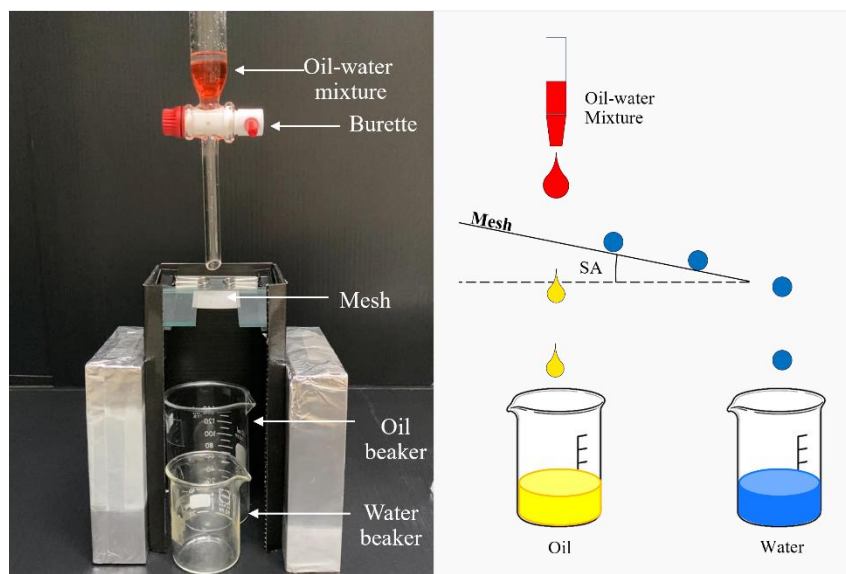
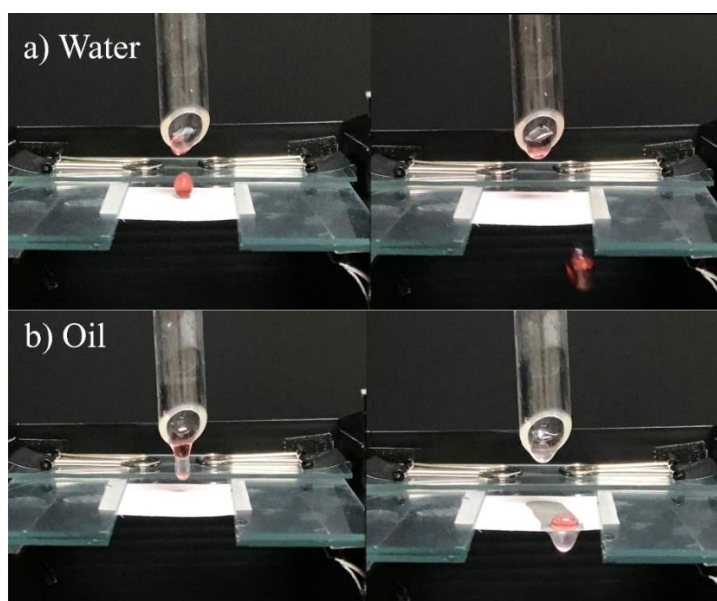


Figure 4.14

Still Photographs of Water and Oil Being Separated Through a PDMS-SiO₂ Coated Stainless-Steel Mesh



Note. This image is an experiment of water and mineral oil separation. a) water (red) being rolled-off from the mesh and b) oil (white) being separated through the mesh.

Table 4. 1

Data of Water Inserted and Collected with Different Types of Oil & Their Respective Separation Efficiency

Type of oil	Water inserted (g)	Water collected (g)			Efficiency (%)		
		PDMS-SiO ₂ coated mesh			PDMS-SiO ₂ coated mesh		
		0.5 ml	1.0 ml	1.5 ml	0.5 ml	1.0 ml	1.5 ml
Cooking oil	4	3.7110	3.6483	3.7237	92.78	91.21	93.09
Disel B7	4	3.6471	3.7304	3.6504	91.18	93.26	91.26
Gasohol 95	4	3.7291	3.6450	3.7253	93.23	91.12	93.13
Mineral oil	4	3.6508	3.7262	3.6470	91.27	93.16	91.17
Hexane	4	3.7270	3.6512	3.7292	93.18	91.28	93.23
Toluene	4	3.6403	3.7172	3.6399	91.01	92.93	91.00

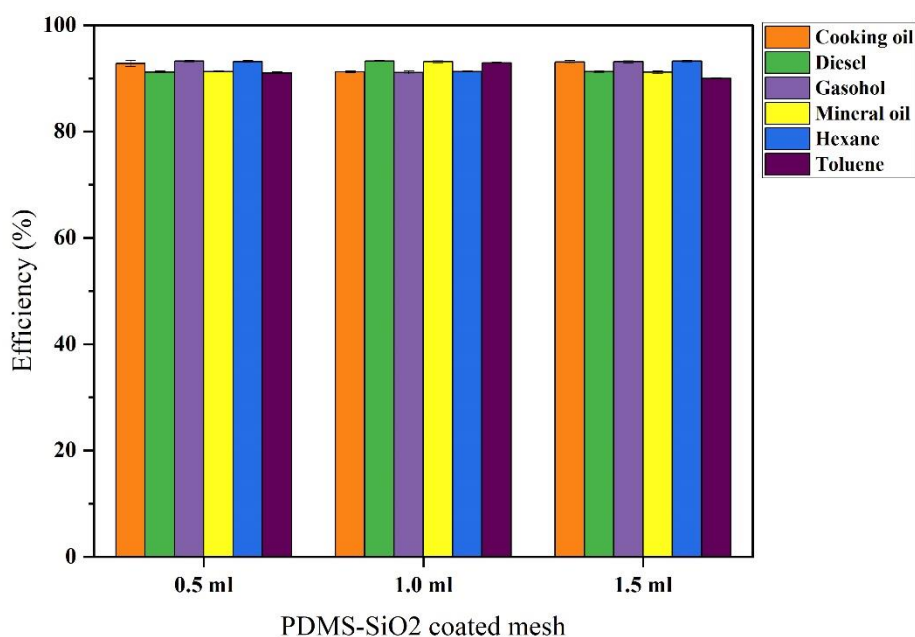
The amount of water collected after the separation test for each oil type (cooking oil, diesel B7, gasohol 95, mineral oil, hexane, and toluene) and their respective separation efficiencies are shown in Table 4.1 above. The effectiveness of the superhydrophobic PDMS-SiO₂ coated mesh is expressed in percent separation efficiency. For this various oil types (cooking oil, diesel B7, gasohol 95, mineral oil, hexane, and toluene) were added to water to achieve an oil-water mixture containing a 1:4 w/w ratio of oil to water. The separation efficiency, determined by the recovered water mass compared to the initial water mass, varied depending on the oil type and the mesh coating amount (0.5 , 1.0, and 1.5 ml). As shown in the table 4.1, efficiencies ranged between 91% to 93% for most of the oil-water combinations.

These variations in separation efficiency can be attributed to two key factors. Firstly, oil properties, namely viscosity and surface tension of the oil influence its interaction with the mesh and water. Less viscous oils can flow through the mesh pores more readily, potentially leading to higher efficiencies. Conversely, oils with lower surface tension can spread more on the mesh surface, hindering water flow, and reducing efficiency.

The second factor is the mesh properties. The PDMS-SiO₂ coating thickness affects the mesh's porosity, pore size distribution, and surface roughness. A well-designed mesh should allow oil to pass through efficiently while retaining water at the surface due to its superhydrophobic and oleophilic properties. The findings of the oil-water separation test revealed small variations in the oil-water separation efficiencies for the PDMS-SiO₂ coated mesh with respect to their volume sprayed to construct the superhydrophobic mesh.

Figure 4.15

Influence of PDMS-SiO₂ Coating on the Oil-Water Separation Capacity of Meshes



Based on the results as shown in Figure 4.15, it appears that PDMS-SiO₂ coated mesh filters with coating volumes of either 0.5 ml or 1.5 ml are suitable for separating water efficiently from certain oil types, particularly cooking oil, gasohol, and hexane. These combinations achieved separation efficiencies consistently around 93%, indicating effective separation of a significant portion of water from the oil.

However, for other oil types like diesel, mineral oil, and toluene, the 1.0 ml PDMS-SiO₂ coating showed 93% efficient separation. The filters with this coating volume exhibited a trend of slightly higher recovered water amounts compared to the 0.5 ml and 1.5 ml coatings for these specific oil types. However, it should be noted that for all oil types the separation efficiencies are consistently within 90-93% irrespective of the volume of PDMS-SiO₂ used, suggesting that the amount of PDMS-SiO₂ used to prepare the superhydrophobic mesh has minimal effect on their oil-water separation efficiency.

CHAPTER 5

CONCLUSION

In conclusion, this study successfully fabricated superhydrophobic meshes coated with PDMS-SiO₂ composites which has a WCA value of approximately 155° and an SA of approximately 7°. The oil contact angle measurements demonstrated their exceptional oil repellency, making them suitable for applications requiring oil-water separation or oil droplet manipulation.

Durability tests revealed the remarkable resilience of PDMS-SiO₂ coatings against mechanical stress compared to uncoated and pure PDMS counterparts. pH stability analysis indicated minimal influence of water pH on their hydrophobicity, ensuring consistent performance under various environmental conditions.

The self-cleaning test highlighted the superior ability of PDMS-SiO₂ coatings to remove contaminants due to their superhydrophobic and low surface energy properties. This characteristic makes them ideal for applications where self-cleaning functionality is crucial.

Finally, the efficiency test explored the effectiveness of these meshes in separating water from different oil types with separation efficiency consistently above 90%. The results suggest that both coating volume and oil properties play a role in separation performance. Identifying the optimal coating thickness for specific oil types can further enhance separation efficiency.

Overall, this research demonstrates the promising potential of PDMS-SiO₂ coated meshes for various applications requiring durability, self-cleaning functionality, and efficient oil-water separation.

For recommendation on this research, future efforts should focus on optimizing the PDMS-SiO₂ composite for even better repellency and efficiency, exploring upscaling

production for large-scale use, and testing the filter's performance in real-world scenarios. To maximize practical impact, the filter can be developed commercially for industrial oil-water separation, environmental cleanup of oil spills, and even separating oil and water byproducts in the food and beverage industry. However, further investigation is needed regarding cost-effectiveness compared to existing methods and the environmental impact of the filter material throughout its lifecycle.

REFERENCES

- Bartolo, D., Bouamirrene, F., Verneuil, É., Buguin, A., Silberzan, P., & Moulinet, S. (2006). Bouncing or sticky droplets: Impalement transitions on superhydrophobic micropatterned surfaces. *Europhysics Letters*, *74*(2), 299–305. <https://doi.org/10.1209/epl/i2005-10522-3>
- Chen, C., Weng, D., Mahmood, A., Chen, S., & Wang, J. (2019). Separation Mechanism and Construction of Surfaces with Special Wettability for Oil/Water Separation. *ACS Applied Materials and Interfaces*, *11*(11), 11006–11027. <https://doi.org/10.1021/acsami.9b01293>
- Chu, Z., Feng, Y., & Seeger, S. (2015). Oil/water separation with selective superantiwetting/superwetting surface materials. *Angewandte Chemie - International Edition*, *54*(8), 2328–2338. <https://doi.org/10.1002/anie.201405785>
- Duta, L., Popescu, A. C., Zgura, I., Preda, N., & Mihailescu, I. N. (2015). Wettability of Nanostructured Surfaces. In *Wetting and Wettability*. InTech. <https://doi.org/10.5772/60808>
- Gabor L. Hornyak, J. D. H. F. T. etc. (2008). *Introduction to Nanoscience*. 297–306.
- Ge, D., Yang, L., Zhang, Y., Rahmawan, Y., & Yang, S. (2014). Transparent and superamphiphobic surfaces from one-step spray coating of stringed silica nanoparticle/sol solutions. *Particle and Particle Systems Characterization*, *31*(7), 763–770. <https://doi.org/10.1002/ppsc.201300382>
- GmbH, K. (2012). *Roll-Off of Sliding Angle and Dynamic Contact Angles Drop Shape Analyzer-DSA100 Drop Shape Analyzer-DSA30*. www.kruss.de
- Gong, X., & He, S. (2020). Highly Durable Superhydrophobic Polydimethylsiloxane/Silica Nanocomposite Surfaces with Good Self-Cleaning Ability. *ACS Omega*, *5*(8), 4100–4108. <https://doi.org/10.1021/acsomega.9b03775>
- Gupta, R. K., Dunderdale, G. J., England, M. W., & Hozumi, A. (2017). Oil/water separation techniques: A review of recent progresses and future directions. In *Journal of Materials Chemistry A* (Vol. 5, Issue 31, pp. 16025–16058). Royal Society of Chemistry. <https://doi.org/10.1039/c7ta02070h>

- ITOPF. (2024, April 18). *Oil Tanker Spill Statistics 2023*.
<https://www.itopf.org/knowledge-resources/data-statistics/statistics/>
- Kumar, A., & Nanda, D. (2019). Methods and fabrication techniques of superhydrophobic surfaces. In *Superhydrophobic Polymer Coatings: Fundamentals, Design, Fabrication, and Applications* (pp. 43–75). Elsevier. <https://doi.org/10.1016/B978-0-12-816671-0.00004-7>
- Lafuma, A., & Quéré, D. (2003). Superhydrophobic states. In *Nature Materials* (Vol. 2, Issue 7, pp. 457–460). <https://doi.org/10.1038/nmat924>
- Li, J., Yan, L., Li, H., Li, J., Zha, F., & Lei, Z. (2015). A facile one-step spray-coating process for the fabrication of a superhydrophobic attapulgite coated mesh for use in oil/water separation. *RSC Advances*, 5(66), 53802–53808. <https://doi.org/10.1039/c5ra08478d>
- Rao, P. A. (2019). *Fabrication of Titanium Dioxide Coated Stainless Steel Mesh Filters for Oil/Water Separation*.
- Reyssat, M., Pépin, A., Marty, F., Chen, Y., & Quéré, D. (2006). Bouncing transitions on microtextured materials. *Europhysics Letters*, 74(2), 306–312. <https://doi.org/10.1209/epl/i2005-10523-2>
- Reyssat, M., Yeomans, J. M., & Quéré, D. (2008). Impalement of fakir drops. *EPL*, 81(2). <https://doi.org/10.1209/0295-5075/81/26006>
- R.N. Wenzel. (1936). *Theory of Wetting Action at Solid Surfaces*.
- Shen, Y., Li, K., Chen, H., Wu, Z., & Wang, Z. (2021). Superhydrophobic F-SiO₂@PDMS composite coatings prepared by a two-step spraying method for the interface erosion mechanism and anti-corrosive applications. *Chemical Engineering Journal*, 413. <https://doi.org/10.1016/j.cej.2020.127455>
- Tanujjal Bora. (2022). *Nanosurface-surface-area-surface-energy*.
- Wang, Y., Liu, Z., Wei, X., Liu, K., Wang, J., Hu, J., & Lin, J. (2021). An integrated strategy for achieving oil-in-water separation, removal, and anti-oil/dye/bacteria-fouling. *Chemical Engineering Journal*, 413. <https://doi.org/10.1016/j.cej.2020.127493>
- Wu, Y., Jia, S., Wang, S., Qing, Y., Yan, N., Wang, Q., & Meng, T. (2017). A facile and novel emulsion for efficient and convenient fabrication of durable superhydrophobic materials. *Chemical Engineering Journal*, 328, 186–196. <https://doi.org/10.1016/j.cej.2017.07.023>

- Xue, Z., Cao, Y., Liu, N., Feng, L., & Jiang, L. (2014). Special wettable materials for oil/water separation. In *Journal of Materials Chemistry A* (Vol. 2, Issue 8, pp. 2445–2460). <https://doi.org/10.1039/c3ta13397d>
- Zhang, N., Qi, Y., Zhang, Y., Luo, J., Cui, P., & Jiang, W. (2020). A review on oil/water mixture separation material. In *Industrial and Engineering Chemistry Research* (Vol. 59, Issue 33, pp. 14546–14568). American Chemical Society. <https://doi.org/10.1021/acs.iecr.0c02524>
- Zhang, N., Yang, X., Wang, Y., Qi, Y., Zhang, Y., Luo, J., Cui, P., & Jiang, W. (2022). A review on oil/water emulsion separation membrane material. *Journal of Environmental Chemical Engineering*, 10(2). <https://doi.org/10.1016/j.jece.2022.107257>
- Zhong, M., Zhang, Y., Li, X., & Wu, X. (2018). Facile fabrication of durable superhydrophobic silica/epoxy resin coatings with compatible transparency and stability. *Surface and Coatings Technology*, 347, 191–198. <https://doi.org/10.1016/j.surfcoat.2018.04.063>
- Zhu, Z., Merlin, F., Yang, M., Lee, K., Chen, B., Liu, B., Cao, Y., Song, X., Ye, X., Li, Q. K., Greer, C. W., Boufadel, M. C., Isaacman, L., & Zhang, B. (2022). Recent advances in chemical and biological degradation of spilled oil: A review of dispersants application in the marine environment. *Journal of Hazardous Materials*, 436. <https://doi.org/10.1016/j.jhazmat.2022.129260>